Site-Hopping Dynamics of Benzene Adsorbed on Ca-LSX Zeolite Studied by Solid-State Exchange ^{13}C NMR

D. J. Schaefer,[†] D. E. Favre,[†] M. Wilhelm,[§] S. J. Weigel,[‡,∥] and B. F. Chmelka*,[†]

Contribution from the Departments of Chemical Engineering and Chemistry, University of California, Santa Barbara, California 93106

Received May 14, 1997[⊗]

Abstract: First-time applications of solid-state exchange ^{13}C NMR techniques to the study of the reorientation dynamics of hydrocarbon molecules adsorbed on zeolites have enabled the geometry and time scales of molecular hopping processes between adjacent adsorption sites to be characterized directly and model free. Two-dimensional exchange ^{13}C NMR on static samples establishes the geometry of the site-hopping dynamics, while one-dimensional magic-angle spinning (MAS) exchange-induced-sidebands (EIS) ^{13}C NMR permits motional correlation times on the order of milliseconds to seconds to be extracted directly from the experimental data. Variable-temperature experiments performed on Ca-LSX zeolite samples with average bulk loadings of 0.5, 1, and 2 benzene molecules per supercage yield apparent Arrhenius activation energies of about 66 ± 6 kJ mol^{-1} for the discrete, localized reorientation dynamics of benzene molecules among different Ca^{2+} cation adsorption sites (∼0.5 nm apart). Arrhenius preexponential factors were established to be on the order of 1×10^{12} s^{-1}, consistent with elementary hopping processes. Motional correlation times exhibit only minor variations upon changes in benzene loading over the range studied.

Introduction

Zeolites are nanoporous aluminosilicates comprised of an extended network of TO_4 tetrahedra (T = Si, Al) that are arranged into three-dimensional crystalline frameworks with molecule-sized channels or cavities and large internal surface areas.[1−3] Zeolites are used in a wide range of commercially important applications, including separations, adsorption, and catalysis, where the transport behaviors of molecular guest species inside the host matrices play central roles in material and process functions.[4,5] Understanding the molecular origins of the macroscopic transport properties of these complicated heterogeneous systems is crucial to establishing and controlling key materials and process parameters, with the goal of improving adsorption, diffusion, and reaction performance of nanoporous solids.

Ca-LSX, $(AlO_2)_{96}(SiO_2)_{96}Ca_{48}$, a faujasite-type zeolite,[6] is closely related to commercial nanoporous molecular sieves used widely as adsorbents and catalysts in hydrocarbon processing and in air separation. The selection of the benzene/Ca-LSX system for this first comprehensive investigation was based on several factors, including the industrial importance of faujasite-type zeolites and the ordered framework of the LSX structure, which reduces the effects of structural disorder and cation distributions on adsorbate dynamics. In addition, the temperature dependence of the spin-echo ^2H NMR line shape of perdeuterated benzene, $C_6{}^2H_6$, adsorbed on Ca-LSX indicated that the site-hopping motions of benzene possessed correlation times at room temperature suitable for exchange NMR, namely 10^{-3} s $< \tau_c < 10^2$ s.[7]

The faujasite structure is one of the numerous known zeolite framework topologies and has a unit cell with 192 tetrahedral units, a portion of which is represented by the single supercage shown in Figure 1a.[1] A purely siliceous faujasite structure is represented by the formula $(SiO_2)_{192}$ and has an electrically neutral framework; each aluminum substitution, up to an apparent maximum of 50% of the tetrahedral framework sites (governed by Loewenstein's rule),[8] gives rise to a negative charge on the framework that must be balanced by extraframework cations. The zeolite compositions obtained by the substitution of aluminum for silicon in the faujasite framework have been given different names according to their Si/Al ratio: zeolite Y for Si/Al > 1.5, zeolite X for 1 < Si/Al ≤ 1.5, and LSX (low-silica X) for Si/Al = 1. The number and location of AlO_4 tetrahedra affect the number and placement of such cations, contributing to the structural heterogeneity of the zeolite. By Loewenstein's rule,[8] the LSX framework represents the faujasite structure with the maximum framework aluminum content, consisting of highly ordered alternating SiO_4 and AlO_4 tetrahedra. Cation siting in dehydrated Ca-LSX has been determined from powder X-ray and neutron diffraction.[7] The Ca^{2+} cations are located preferentially in sites SI and sites SII, with no evidence found for the presence of cations in SIII positions, see Figure 1a. The four SII sites within each supercage are arranged tetrahedrally; inverting this tetrahedron gives the arrangement of the four windows connecting adjacent supercages, two of which are shown in Figure 1b. Because the supercages are arranged on a diamond lattice, the corresponding SII and window sites within a LSX crystallite are at angles of 0°, 70.5°, 109.5°, or 180° relative to each other.

The extraframework cations occupy distinct positions inside the dehydrated zeolite cavities and represent energetically preferred sites for adsorption of molecular guest species on the

[†] Department of Chemical Engineering.
[‡] Department of Chemistry.
[§] Present address: Max-Planck-Institut für Polymerforschung, D-55021 Mainz, Germany.
[∥] Present address: Air Products and Chemicals, Inc., Allentown, PA 18195.
[⊗] Abstract published in *Advance ACS Abstracts,* September 1, 1997.

(1) Breck, D. W. *Zeolite Molecular Sieves*; Krieger: Malabar, 1974.
(2) Jansen, J. C., Stöcker, M., Karge, H. G., Weitkamp, J., Eds. *Advanced Zeolite Science and Applications*; Elsevier Science B.V.: Amsterdam, 1994.
(3) Weitkamp, J., Karge, H. G., Pfeifer, H., Hölderich, W., Eds. *Zeolites and Related Microporous Materials: State of the Art 1994*; Elsevier Science B.V.: Amsterdam, 1994.
(4) Chen, N. Y.; Degnan, T. F., Jr.; Smith, C. M. *Molecular Transport and Reaction in Zeolites*; VCH Publishers, Inc.: New York, 1994.
(5) Kärger, J.; Ruthven, D. M. *Diffusion in Zeolites and Other Microporous Solids*; Wiley: New York, 1992.
(6) Meier, W. M.; Olson, D. H.; Baerlocher, C. *Atlas of Zeolite Structure Types,* 4th ed.; Butterworth-Heinemann: Boston, 1996.
(7) Vitale, G.; Bull, L. M.; Morris, R. E.; Cheetham, A. K.; Toby, B. H.; Coe, C. G.; MacDougall, J. E. *J. Phys. Chem.* **1995**, *99*, 16087−16092.
(8) Loewenstein, W. *Am Mineral.* **1954**, *39*, 92−96.

S0002-7863(97)01563-1 CCC: $14.00 © 1997 American Chemical Society

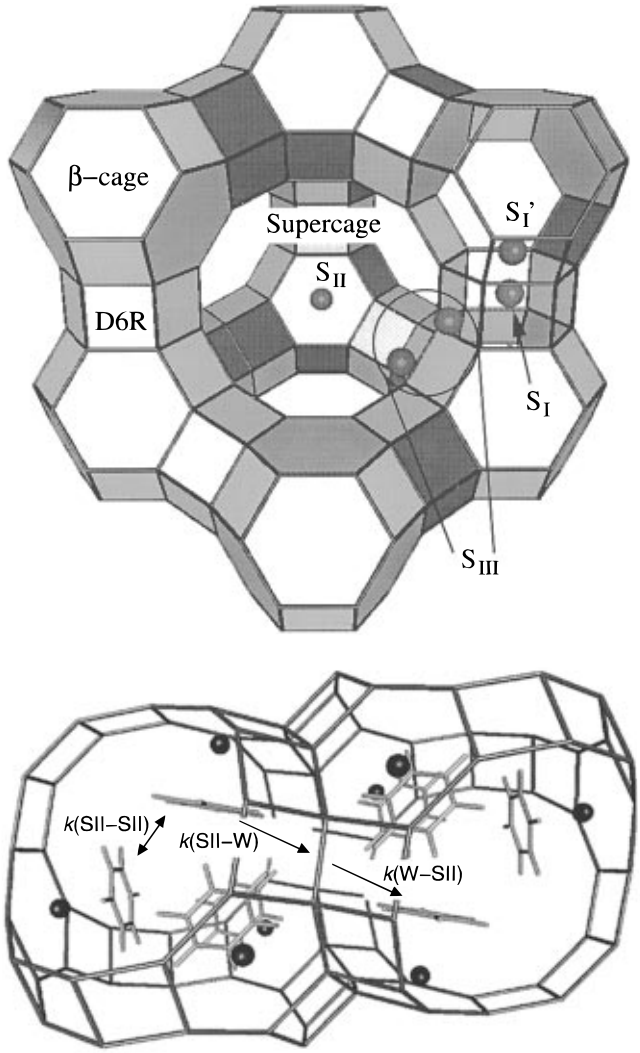

Figure 1. (a, top) Schematic drawing of the faujasite structure with extraframework cation sites shown. Tetrahedrally coordinated Si or Al atoms are located at vertices and bridging oxygen atoms are represented as the connecting lines. The SI site is located at the center of the double 6-ring units (D6R) connecting the sodalite (β) cages. The SI′ site lies out of the plane of one of the 6-rings of the D6R unit and projects into the β-cage. Because of the close proximity of SI′ to SI, the two positions may not be occupied simultaneously. The SII site is located outside and above a 6-ring of the sodalite cage and is accessible to adsorbing species within the supercage (α-cage). The site designated SII′ is located inside the sodalite cages on the opposite side of the 6-ring from the SII site. Finally, the SIII position lies in the supercage above the 4-rings and adjacent to the 12-ring window. Supercage cavities are ∼1.3 nm in diameter and are connected via ∼0.74-nm diameter windows; there are eight such cavities in the unit cell. (b, bottom) Benzene molecules adsorbed at SII cation sites in Ca-LSX. Benzene molecules fit only through the 12-ring windows and into the supercage cavities of the faujasite structure, where they can adsorb at a SII cation site facially coordinated to the cation. At higher concentrations of benzene, a second adsorption site may be occupied in the plane of the 12-ring window (W) joining adjacent supercages. Also indicated are three of the four fundamental rate coefficients k(SII→SII), k(SII→W), k(W→SII), and k(W→W) for intra- and intercage motion of benzene molecules inside the supercages of the zeolite.

heterogeneous internal zeolite surface.[1] The adsorption of benzene in faujasite-type zeolites has been extensively investigated by a variety of techniques. Due to its 0.6 nm diameter, a benzene molecule cannot fit into all regions of the porous faujasite structure; for example, calcium cations at the SI and SI′ sites shown in Figure 1a are inaccessible to adsorbing benzene species. However, benzene does fit through the 12-ring windows (0.74 nm diameter) and in the supercage cavities, where an adsorption site exists above each SII cation to which an adsorbed benzene molecule will be facially coordinated, as shown in Figure 1b. Previous ^{1}H and ^{2}H NMR studies[9,10] have established a rapid rotation about the C_6 axis of adsorbed benzene coordinated to an SII site cation even at low temperatures (<100 K). At higher concentrations of benzene (2.6 molecules per supercage in Na-Y), neutron diffraction investigations[11] have revealed a second adsorption site at the center of the 12-ring window (W) adjoining two supercages, such as those portrayed in Figure 1b. Infrared[12] and Raman spectroscopy[13] investigations have provided supporting evidence for such a site at similar concentration levels of the adsorbate. The heat of adsorption at low benzene loadings in Ca-X (Si/Al ratio = 1.17) is −134 kJ mol^{-1}, as given by the isosteric enthalpy of adsorption.[14] This decreases in magnitude to −103 kJ mol^{-1} at a loading of 2.6 to 3 benzene molecules per supercage, apparently because adsorption at window sites becomes important. The maximum possible loading has been documented to be between 5 and 6 benzene molecules per supercage.[14,15]

Experimental probes of guest motion over molecular length scales have proven difficult in these heterogeneous systems, but are essential for understanding diffusion of guest species within the intracrystalline zeolite channels. In particular, molecular-hopping dynamics between discrete adsorption sites are central to diffusion over longer length scales, which arises from a series of many such nanoscale hopping events. Extensive computer simulations on zeolites, aimed at studying the sorptive behavior of guest molecules, have provided a detailed picture of the structure inside the zeolite cavities and of the dynamics of single molecules.[16] In addition, the dynamics and the diffusional behavior of guest molecules in zeolites have been widely studied by molecular dynamics (MD) and Monte Carlo (MC) simulations.[17] The objectives of these simulations are to explain and predict molecular and macroscopic diffusion measurements, for which it is especially important to distinguish experimentally between intracage and intercage mobilities of guest molecules. Only results that relate specifically to cage-to-cage migration are directly relevant to macroscopic diffusivity measurements.

Experimental methods available to study diffusion on macroscopic length scales (>1 μm) include pulsed-field-gradient (PFG) NMR,[18] adsorption uptake, zero-length column (ZLC) chromatography techniques, and tracer measurements.[4,5,19] By comparison, quasi-elastic neutron scattering (QENS),[20] spin−echo ^{2}H NMR line-shape analysis,[21] spin−spin (T_2) and spin−lattice (T_1) NMR relaxation measurements[22] are sensitive to

(9) Lechert H.; Wittern, K.-P. *Ber. Bunsen-Ges. Phys. Chem.* **1978**, *82*, 1054−1060.
(10) Burmeister, R.; Schwarz H.; and Boddenberg, B. *Ber. Bunsen-Ges. Phys. Chem.* **1989**, *93*, 1309−1313.
(11) Fitch, A. N.; Jobic, H.; Renouprez, A. *J. Phys. Chem.* **1986**, *90*, 1311−1318.
(12) de Mallmann, A.; Barthomeuf, D. *J. Chem. Soc., Chem. Commun.* **1986**, *90*, 476−477.
(13) Freeman, J. J.; Unland, M. L. *J. Catal.* **1978**, *54*, 183−196.
(14) Blank, H.; Bülow, M.; Schirmer, W. *Z. Phys. Chem.* **1979**, *260*, 395−402.
(15) Liu, S.-B.; Ma, L.-J.; Lin, M.-W.; Wu, J.-F.; Chen, T.-L. *J. Phys. Chem.* **1992**, *96*, 8120−8125.
(16) Catlow, C. R. A., Ed. *Modelling of Structure and Reactivity in Zeolites*; Academic Press: San Diego, 1992.
(17) (a) Henson, N. J.; Cheetham, A. K. *J. Inclusion Phenom. Mol. Recognit. Chem.* **1995**, *21*, 137−158. (b) Auerbach, S. M.; Metiu, H. I. *J. Chem. Phys.* **1997**, *106*, 2893−2905. (c) Auerbach, S. M.; Metiu, H. I. *J. Chem. Phys.* **1996**, *105*, 3753−3760. (d) Auerbach, S. M.; Henson, N. J.; Cheetham, A. K.; Metiu, H. I. *J. Phys. Chem.* **1995**, *99*, 10600−10608. (e) Keffer, D.; McCormick, A. V.; Davis, H. T. *J. Phys. Chem.* **1996**, *100*, 967−973. (f) Klein, H.; Kirschhock, C.; Fuess, H. *J. Phys. Chem.* **1994**, *98*, 12345−12360. (g) Klein, H.; Fuess, H.; Schrimpf, G. *J. Phys. Chem.* **1996**, *100*, 11101−11112.

motions occurring on molecular length scales. Relaxation time measurements, however, rely on model assumptions to relate experimentally obtained parameters to motional correlation times, τ_c, and subsequently to diffusivities. As a result, relaxation time analyses do not distinguish unambiguously between different molecular dynamic processes. As an example, ^{2}H T_1 relaxation time measurements have been widely applied to examine diffusivities and activation energies of benzene dynamics in zeolites.[10,23] Their analyses and interpretations need to account for the rotation of each benzene molecule about its 6-fold axis, for the librational motion of the 6-fold axis, and finally for molecular hopping among adsorption sites to connect the measured T_1 values with a motional correlation time τ_c for the site-hopping motion.[24] Spin−lattice relaxation time measurements, however, lack the sensitivity necessary to distinguish among competing motional processes, because the relation between motional correlation times and T_1 values depends only on the spectral density, that is, the half-sided Fourier-transform of the second-order orientational autocorrelation function $C_2(t)$ of the motional process at and at twice the Larmor frequency.[25]

In contrast, two-dimensional (2D) exchange NMR experiments can yield geometric and time scale information directly from the experimental data without the need of a model for the motional process and without further knowledge of sample-related parameters.[26] In fact, all even-order orientational autocorrelation functions $C_L(t)$, $L = 2, 4$, etc., can be calculated directly from experimental 2D exchange spectra. Multidimensional exchange NMR and, in particular, 2D exchange NMR[27] techniques provide powerful means for probing dynamics on molecular (1 nm) length scales, as demonstrated convincingly in the study of reorientation geometries and time scales of slow dynamic processes in polymers.[26] Two-dimensional exchange ^{129}Xe NMR[28] and related one-dimensional DANTE exchange ^{129}Xe NMR experiments[29] have been applied to study cage-to-cage migration of xenon atoms physically adsorbed on Na-A zeolite, relying on high intracage mobility of the xenon atoms to produce narrow isotropic NMR lines. Variable-temperature experiments yielded an activation energy of about 60 ± 10 kJ mol^{-1} for the transfer of a xenon atom from one cage to another.[28] Two-dimensional exchange ^{129}Xe NMR has also been used to obtain the rate coefficients for intercrystalline xenon exchange in physical mixtures of Na-X and Na-Y zeolite powders, which have yielded Arrhenius activation energies of 3.6 and 4.4 kJ mol^{-1} for xenon exchange in Na-X and Na-Y, respectively.[30] While QENS, spin-echo NMR line shapes, T_1 and T_2 NMR relaxation, and exchange NMR methods all provide means to determine time scales of guest dynamics, insights on the geometries of motional processes are provided by QENS, 2D exchange NMR and related time-domain echo techniques, the newly developed 3D DIfference-COrrelated (DICO) experiment,[31] and to a lesser extent, spin−echo NMR line-shape analyses. The various techniques, furthermore, probe complementary motional time scales, namely 10^{-12} s $< \tau_c < 10^{-8}$ s for QENS, 10^{-6} s $< \tau_c < 10^{-4}$ s for spin−echo NMR line-shape analyses, and 10^{-3} s $< \tau_c < 10^2$ s for 2D exchange NMR and related exchange NMR techniques.

Recently, we demonstrated the feasibility of solid-state 2D exchange ^{13}C NMR methods for investigating the molecular transport dynamics of guest species adsorbed on a nanoporous zeolite host, specifically benzene adsorbed on zeolite Ca-LSX.[32] Elliptical off-diagonal intensity patterns in 2D exchange ^{13}C NMR spectra indicated that benzene molecules adsorbed at Ca^{2+} cation sites underwent discrete reorientations through an angle of 109° between adjacent adsorption sites on a time scale on the order of 100 ms at ambient temperature. Here, we present a comprehensive variable-temperature study that provides the first direct correlation time and activation energy measurements of benzene molecules exchanging dynamically among different adsorption sites, along with a more detailed examination of the geometrical aspects of the site-hopping dynamics. Importantly, precise and accurate information on the time scale of the molecular dynamics is obtained directly and model-free from experimental data using a one-dimensional technique, exchange-induced sidebands[33] (EIS) on a sample spinning slowly at the magic angle. Distributions of reorientation angles are found to characterize the geometry of the benzene site-hopping motion and are quantified by examining the final-state structure factor extracted from time-domain stimulated echo signals. The combined applications of complementary exchange NMR techniques to the study of molecular guest dynamics in zeolitic materials yields for the first time direct molecular-level information on geometries and time scales of hydrocarbon transport in porous solids.

Experimental Section

Synthesis. The parent Na,K-LSX zeolite was prepared using the gel composition $6.2Na_2O:1.5K_2O:2SiO_2:Al_2O_3:124H_2O$. Sodium aluminate, NaOH, and KOH were dissolved in deionized water before being added to the appropriate amount of a colloidal suspension of SiO_2 in water that was stabilized to remain in solution with a small amount of sodium cations (Ludox LS-30, Dupont). The resulting gel was stirred in a glass beaker at 313 K for 3 days. After the sample appeared fully crystalline, it was recovered by vacuum filtration, washed with deionized water, rinsed with acetone, and dried under ambient

(18) (a) Kärger, J.; Pfeifer, H.; Heink, W. *Adv. Magn. Reson.* **1988**, *12*, 1−89. (b) Bell, A. T., Pines, A., Eds. *NMR Techniques in Catalysis*; Marcel Dekker, Inc.: New York, 1994.

(19) Ruthven, D. M. *Principles of Adsorption and Adsorption Processes*; Wiley: New York, 1984.

(20) Bée, M. *Quasielastic Neutron Scattering, Principles and Applications in Solid State Chemistry, Biology and Materials Science*; Adam Hilger: Philadelphia, 1988.

(21) Gladden, L. F. *Chem. Eng. Sci.* **1994**, *49*, 3339−3408.

(22) (a) Pfeifer, H. *NMR Basic Principles and Progress*; Springer Verlag: New York, 1972; Vol. 7, pp 53−153. (b) Tycko, R. *Nuclear Magnetic Resonance Probes of Molecular Dynamics*; Kluwer Academic Publishers: Boston, 1994.

(23) (a) Bull, L. M.; Henson, N. J.; Cheetham, A. K.; Newsam, J. M.; Heyes, S. J. *J. Phys. Chem.* **1993**, *97*, 11776−11780. (b) Auerbach, S. M.; Bull, L. M.; Henson, N. J.; Metiu, H. I.; Cheetham, A. K. *J. Phys. Chem.* **1996**, *100*, 5923−5930. (c) Voss, V.; Boddenberg, B. *Surf. Sci.* **1993**, *298*, 241-250. (d) Sousa Gonçalves, J. A.; Portsmouth, R. L.; Alexander, P.; Gladden, L. F. *J. Phys. Chem.* **1995**, *99*, 3317−3325. (e) Alexander, P.; Gladden, L. F. *Zeolites* **1997**, *18*, 38−43.

(24) (a) Boddenberg, B.; Burmeister, R. *Zeolites* **1988**, *8*, 488-494. (b) Boddenberg, B.; Beerwerth, B. *J. Phys. Chem.* **1989**, *93*, 1440−1447.

(25) Spiess, H. W. *NMR Basic Principles and Progress*; Springer Verlag: Berlin, 1978; Vol. 15 pp 59−210.

(26) Schmidt-Rohr, K.; Spiess, H. W. *Multidimensional Solid-State NMR and Polymers*; Academic Press: San Diego, 1994.

(27) Ernst, R. R.; Bodenhausen, G.; Wokaun, A. *Principles of Nuclear Magnetic Resonance in One and Two Dimensions*; Clarendon Press: Oxford, 1987.

(28) (a) Larsen, R. G.; Shore, J.; Schmidt-Rohr, K.; Emsley, L.; Long, H.; Pines, A.; Janicke, M.; Chmelka, B. F. *Chem. Phys. Lett.* **1993**, *214*, 220−226. (b) Janicke, M.; Chmelka, B. F.; Larsen, R. G.; Shore, J.; Schmidt-Rohr, K.; Emsley, L.; Long, H.; Pines, In *Zeolites and Related Microporous Materials: State of the Art 1994*; Weitkamp, J., Karge, H. G., Pfeifer, H., Holderich, W., Eds.; Elsevier Science B. V.: Amsterdam, 1994; pp 519−526.

(29) Jameson, A. K.; Jameson, C. J.; Gerald, R. E., II. *J. Chem. Phys.* **1994**, *101*, 1775−1786.

(30) Moudrakovski, I. L.; Ratcliffe, C. I.; Ripmeester, J. A. In *Zeolites: A Refined Tool for Designing Catalytic Sites;* Bonneviot, L., Kaliaguine, S., Eds.; Elsevier Science B.V.: Amsterdam, 1995.

(31) Heuer, A.; Leisen, J.; Kuebler, S. C.; Spiess, H. W. *J. Chem. Phys.* **1996**, *105*, 7088−7096.

(32) Wilhelm, M.; Firouzi, A.; Favre, D. E.; Bull, L. M.; Schaefer, D. J.; Chmelka, B. F. *J. Am. Chem. Soc.* **1995**, *117*, 2923−2924.

(33) Yang, Y.; Schuster, M.; Blümich, B.; Spiess, H. W. *Chem. Phys. Lett.* **1987**, *139*, 239−243.

conditions. The powder X-ray diffraction pattern of the as-synthesized white powder showed that the material possessed a faujasite structure with no detectable features from impurity phases. The MAS ^{29}Si NMR spectrum of the Na,K-LSX product showed a single narrow (150 Hz fwhm at $\omega_R = 2\pi \times 3000$ Hz) resonance at −85 ppm (referenced to TMS), indicating that the material has a Si/Al ratio very close to 1 and is highly ordered. The Na,K-LSX was subsequently ion exchanged six times in 1 M $Ca(NO_3)_2$ solution overnight under reflux conditions (25 mL of exchange solution per gram of wet zeolite). The MAS ^{29}Si NMR spectrum of the fully exchanged Ca-LSX again showed only one narrow resonance (180 Hz fwhm at $\omega_R = 2\pi \times 3000$ Hz) at −85 ppm and one narrow peak (750 Hz fwhm at $\omega_R = 2\pi \times 4000$ Hz) in the MAS ^{27}Al NMR spectrum at 60 ppm (referenced to $Al(NO_3)_3$), indicating that the framework remained highly ordered following ion exchange. Thermal gravimetric analysis revealed that the Ca-LSX sample contains 30.3 wt % water, which is essentially completely removed at 948 K. The degree of calcium ion exchange was greater than 98%, as determined by elemental analysis. The presence of protonated framework defects (terminal Si−OH and Al−OH) was determined by diffuse reflectance infrared spectroscopy and ^{1}H NMR on a sample dehydrated under vacuum ($<10^{-3}$ Pa) at 673 K. The infrared spectrum (4 cm^{-1} resolution) showed four weak but well-resolved peaks in the hydroxyl stretch region at 3514, 3617, 3690, and 3742 cm^{-1}. The first two signals are too shifted to be due to acid protons (as in H−Y) and likely result from $CaOH^+$ species; the other peaks correspond to terminal Al−OH and terminal Si−OH groups, respectively.[34]

Loading. Each sample was dehydrated under vacuum ($<10^{-3}$ Pa) at 673 K for at least 12 h. A known amount of benzene, ^{13}C-enriched to 99% at a single ring site,[35] was added volumetrically in a glovebox under nitrogen atmosphere; samples with an average bulk loading of approximately 0.5, 1, and 2 benzene molecules per supercage were prepared. After reevacuation while cooling the sample with liquid nitrogen, the sample was sealed in a glass ampule and placed in an oven at 353 K for 12 h to distribute the adsorbate throughout the sample. Uniform macroscopic distribution of the adsorbate was confirmed by coadsorbing ^{129}Xe in natural abundance into a sample containing 2 benzene molecules per supercage and acquiring ^{129}Xe NMR spectra. Only a single peak (400 Hz fwhm) at 125 ppm (referenced to xenon gas at very low pressure[36]) was observed in a spectrum acquired after heating the sample to 353 K for 12 h, consistent with rapid averaging of the physically adsorbed ^{129}Xe probe atoms among supercages containing a macroscopically uniform distribution of benzene molecules.[37] The use of ^{13}C-enriched benzene in the sample, rather than relying on ^{13}C in natural abundance (1.1%), was found to be necessary to ensure sufficient NMR signal intensity to carry out the exchange NMR experiments within a reasonable amount of time. However, ^{13}C-enrichment significantly enhances spin diffusion efficiency (as discussed below) in a system where benzene molecules adsorbed in the same supercage are on average approximately 0.5−0.6 nm apart. In this regard, choosing single-site enriched benzene, rather than enrichment at all six carbon sites, represents a compromise between further enhancement of the NMR signal intensity and unwanted effects arising from ^{13}C−^{13}C homonuclear dipolar couplings (predominantly line splitting and broadening from intramolecular couplings and increased spin diffusion efficiency between different molecules). To prove that the contribution of spin diffusion to the exchange NMR spectra is negligible at elevated temperatures where molecular hopping events between adsorption sites are observed, a sample with an average bulk loading of 2 benzene molecules per supercage was prepared using benzene with ^{13}C in natural abundance.

NMR Experiments. All MAS and EIS experiments were performed in on-resonance mode using a Chemagnetics CMX-180 spectrometer operating at 45.3 MHz for ^{13}C and 180.1 MHz for ^{1}H using 7.5 mm zirconia PENCIL rotors spinning at $\omega_R = 2\pi \times 2200$ Hz. Long-term stability better than ±5 Hz was achieved using a Chemagnetics automatic spinning speed controller. Spectra were acquired at T = 338, 311, 298, 286, 274, 262, 249, 238, 218, and 200 K; the reported temperatures are corrected values based on calibrations with methanol[38] (<311 K) and ethylene glycol[39] (>311 K). The temperature was controlled using a standard control unit from Chemagnetics with the accuracy, stability and reproducibility estimated to be ±1 K. Cross-polarization (CP) MAS spectra were recorded under high-power proton dipolar decoupling (DD) ($2\pi \times 40$ kHz) using the pulse sequence shown in Figure 2a; TOSS (TOtal Suppression of spinning Sidebands) experiments[40] and the EIS experiments were performed by applying the four-pulse TOSS sequence displayed in Figure 2b; the EIS pulse sequence is shown in Figure 2c. The timing of the four pulses of the TOSS sequence has proven crucial for effective suppression the spinning sidebands. Best results were obtained for the following set of parameters: $\tau_1/T_R = 0.1888$, $\tau_2/T_R = 0.2301$, $\tau_3/T_R = 0.8112$, $\tau_4/T_R = 1.7699$, $\tau_5/T_R = 2.0$;[41] the times are measured from the end of the CP sequence and T_R stands for the rotor period $T_R = 2\pi/\omega_R$. The use of six-pulse TOSS sequences,[42] TOSS with composite pulses,[43] or the application of other sideband suppression techniques like SELTICS[44] generally produced no improvement over the four-pulse TOSS sequence described above. Phase cycling of the TOSS sequence, however, was essential to achieve good sideband suppression;[26,45] for the EIS experiment the phase cycling was modified to include axial peak suppression. Usually 750 complex points with a dwell time of 15 μs were acquired and zero-filled to 2048 points prior to Fourier transformation. The $\pi/2$-pulse lengths for ^{13}C and ^{1}H ranged between 4.5 and 5 μs, while contact times were 1.5 ms; recycle delays varied between 20 and 30 s. Typical EIS measuring times for a sample with an average bulk loading of 0.5 ^{13}C-enriched benzene molecules per supercage were less than 2 h. Mixing times of approximately t_m = 3, 7, 16, 34, 74, 160, 340, 740, 1600, 3440, and 7440 ms were used.[46] The EIS pulse sequence was synchronized with the rotor period to ensure that the mixing time was always an integer multiple of the rotor period (T_R = 454.55 μs).

Static two-dimensional exchange ^{13}C NMR spectra were recorded in off-resonance mode using a standard CP pulse sequence, as shown in Figure 2d, on a Chemagnetics CMX-180 spectrometer. High-power proton decoupling (DD) was applied during the evolution (t_1) and detection (t_2) periods; in some experiments the decoupling was continued during the mixing time (t_m), for periods as long as 300 ms, to render ^{13}C−^{13}C spin diffusion less efficient (see below). A 32-scan phase cycle was used to suppress spectral artifacts, mainly arising from signal contributions created by spin-lattice relaxation during the mixing time.[47] Spectra were acquired at temperatures T = 312, 298, 274, 250, 226, 202, and 177 K, which are corrected values based on a calibration with methanol.[38] The $\pi/2$-pulse lengths for ^{13}C and ^{1}H ranged between 4.5 and 5 μs, while typical CP contact times were between 1.5 ms (>274 K) and 20 ms (<274 K); recycle delays varied between 5 s at low temperatures (<274 K) and 13 s at higher temperatures (>274 K). A typical delay time between the two pulses of the Hahn-echo sequence in the detection period was 60 μs. In the detection period, normally 128 complex points were acquired with a dwell time of 15 μs; 40 points in 30 μs increments were measured in the evolution period. Prior to Fourier transformation, the data array was zero-filled

(34) Rabo, J. A., Ed. *Zeolite Chemistry and Catalysis*; ACS Monograph Series; American Chemical Society: Washington, DC, 1976; pp 118−284.
(35) Benzene 99% ^{13}C-enriched in a single site was purchased from Isotec, 3858 Benner Road; Miamisburg, OH 45342.
(36) Fraissard, J.; Ito, T. *Zeolites* **1988**, *8*, 350−361.
(37) Chmelka, B. F.; Pearson, J. G.; Liu, S. B.; Ryoo, R.; de Menorval, L. C.; Pines, A. *J. Phys. Chem.* **1991**, *95*, 303−310.
(38) Van Greet, A. L. *Anal. Chem.* **1970**, *42*, 679−680.
(39) Kaplan, M. L.; Bovey, F. A.; Cheng, H. N. *Anal. Chem.* **1975**, *47*, 1703−1705.
(40) (a) Dixon, W. T. *J. Magn. Reson.* **1981**, *44*, 220−223. (b) Dixon, W. T. *J. Chem. Phys.* **1982**, *77*, 1800−1809. (c) Raleigh, D. P.; Olejniczak, E. T.; Griffin, R. G. *J. Chem. Phys.* **1988**, *89*,1333−1350.
(41) Lang, S. J. *J. Magn. Reson., Ser. A* **1993**, *104*, 345−346.
(42) Nielsen, N. C.; Bildsøe, H.; Jakobsen, H. J. *J. Magn. Reson.* **1988**, *80*, 149−154.
(43) Hagemeyer, A.; van der Putten, D.; Spiess, H. W. *J. Magn. Reson.* **1991**, *92*, 628−630.
(44) Hong, J.; Harbison, G. S. *J. Magn. Reson., Ser. A* **1993**, *105*, 128−136.
(45) Blümich, B.; Hagemeyer, A.; Schmidt-Rohr, K.; Spiess, H. W. *Ber. Bunsen-Ges. Phys. Chem.* **1989**, *93*, 1189−1193.
(46) Due to technical details of the rotor-synchronization, mixing times can be between 1/2 T_R and 3/2 T_R longer than the values reported; this uncertainty is not important to the data analysis.
(47) Schaefer, D.; Leisen, J.; Spiess, H. W. *J. Magn. Reson., Ser. A* **1995**, *115*, 60−79.

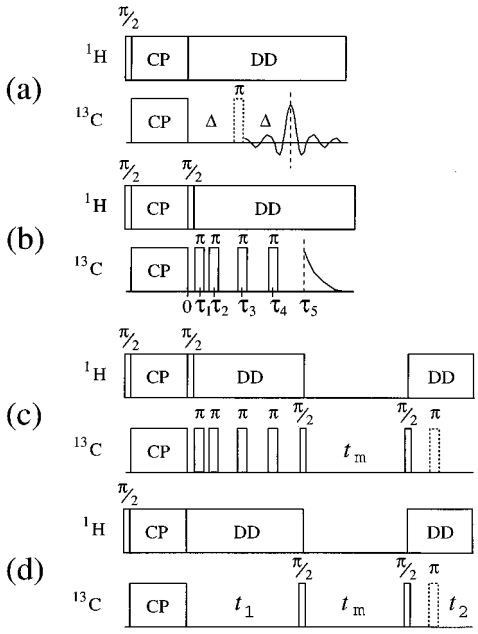

Figure 2. Schematic drawings of the rf-pulse sequences used to measure ^{13}C NMR spectra for systems that are governed by anisotropic chemical-shift interactions. (a) Equivalent to a one-pulse ^{13}C NMR experiment. Transverse proton magnetization is created by a $\pi/2$ proton pulse and is transferred to ^{13}C nuclei by means of cross-polarization (CP). During detection of the FID, high-power proton dipolar decoupling (DD) is applied to remove heteronuclear ^{1}H−^{13}C dipolar couplings. By inserting a refocusing π-pulse a time span Δ after the end of the cross-polarization sequence, a Hahn-echo can be created with a maximum amplitude that occurs at a time Δ after that pulse. For data acquired under MAS conditions, Δ must be an integer multiple of the rotor period T_R, so that the Hahn- and rotor-echoes coincide. (b) Four-pulse TOSS sequence for total suppression of spinning sidebands. Four π-pulses are applied at well-defined times τ_1, τ_2, τ_3, and τ_4 after the cross-polarization period, with detection of the rotor-echo-free FID started at time τ_5 after the last π-pulse. Note that after the CP irradiation, a $\pi/2$ proton pulse is applied to return the proton magnetization back to the z axis to avoid further cross-polarization during the ^{13}C π-pulses. (c) Basic pulse sequence for the exchange-induced-sidebands (EIS) experiment. During the preparation period, the TOSS sequence of Figure 2b is used to suppress spinning sidebands. At the point where the acquisition would begin in a standard TOSS experiment, ^{13}C transverse magnetization is rotated to the z direction by a $\pi/2$-pulse, and a mixing time t_m lasting an integral number of rotor periods begins. At the end of the mixing period, the ^{13}C magnetization is returned to the transverse plane by another $\pi/2$-pulse for detection of the signal. Like in Figure 2a, a Hahn-echo can be created to overcome receiver dead-time effects. The signals of two experiments, which differ only in the phase of the pulse preceding the mixing time, are added to obtain the EIS spectrum. (d) Pulse sequence for two-dimensional (2D) exchange ^{13}C NMR spectra. ^{13}C transverse magnetization is created by cross-polarizing from the protons; the information about the NMR frequencies during the subsequent evolution time t_1 is stored along the z axis by the first $\pi/2$-pulse, which initiates the mixing time t_m. Molecular reorientations can take place during the mixing period, thereby altering the NMR frequencies, which are measured after the second $\pi/2$-pulse in the detection time t_2. Like in Figure 2a, a refocusing π-pulse can be used to create a Hahn-echo in the detection period. A two-dimensional data set $F(t_1,t_2;t_m)$ is generated by repeating the experiment with incremented values of the evolution time t_1 while keeping t_m constant. Fourier transformation with respect to the two times t_1 and t_2 yields the two-dimensional exchange spectrum $S(\omega_1,\omega_2;t_m)$, which correlates the frequencies before and after the mixing time.

to dimensions $(\omega_1 \times \omega_2) = 256 \times 512$. The final spectrum, with a spectral width of $2\pi \times 16.7$ kHz in both dimensions, was obtained by cutting the 2D array to dimensions 128×128 and discarding the $^7/_8$ of the 2D Fourier transform that contains either only baseline (ω_2) or the completely equivalent spectrum in the ω_1 dimension. Typical measuring times to acquire a static 2D exchange ^{13}C NMR spectrum on a sample with two ^{13}C-enriched benzene molecules per supercage were in the range between 5 and 70 h.

Theory

A brief introduction into the NMR experiments used in this study is provided below. For more details on the specific techniques, the reader is referred to ref 48 or, for general background, to NMR texts, such as ref 26.

In the solid state, NMR frequencies depend on the orientations of the molecules in the external magnetic field $\mathbf{B}_0$ due to the anisotropy of the nuclear spin interactions; these orientation-dependent interactions are described by second-rank tensors. The angular dependence of the NMR frequency is then given by

$$\omega' = \omega_0 + {}^1/_2\,\delta\,(3\cos^2\theta - 1 - \eta\sin^2\theta\cos(2\phi)) \quad (1)$$

where ω_0 denotes the Larmor frequency including the isotropic chemical shift, δ specifies the coupling strength, and the asymmetry parameter η represents the deviation from axial symmetry about the z axis of the coupling tensor. The polar angles θ and ϕ describe the orientation of the magnetic field $\mathbf{B}_0$ in the principal axes system of the interaction tensor. The principal axes system for the generally dominating intramolecular interaction contributions is determined by the local symmetry of the molecule in the vicinity of the nucleus under study. In the C_6H_6/Ca-LSX system, benzene molecules adsorbed at Ca^{2+} cation sites spin rapidly about their 6-fold axes, anisotropically averaging the chemical shift tensor of each molecule and yielding a time-averaged ^{13}C spectrum with $\eta = 0$. Therefore, only the angle θ between the z principal axis of the chemical shift tensor (directed in the case of benzene along the 6-fold symmetry axis perpendicular to the ring plane) and the external magnetic field is relevant:

$$\omega = \frac{\omega' - \omega_0}{\delta} = {}^1/_2\,(3\cos^2\theta - 1) = P_2(\cos\theta) \quad (2)$$

where $P_2(\cos\theta)$ is the second-order Legendre polynomial.

Two-Dimensional Exchange NMR. Two-dimensional exchange NMR[27] monitors changes in the angular-dependent NMR frequencies occurring on a time scale ranging from milliseconds to a few seconds during a mixing time (t_m) by correlating the frequencies in the evolution (t_1) and detection (t_2) periods, which bracket the mixing time, see Figure 2d. For characteristic time constants on the order of the mixing time for the process causing such frequency changes, and with the condition $t_m \gg t_1$, t_2, frequencies can be considered constant during the evolution and detection periods and are expected to change (if at all) during the mixing time only. Such changes in the NMR frequencies manifest themselves as off-diagonal intensity in the 2D exchange spectrum $S(\omega_1,\omega_2;t_m)$, which can be regarded as a correlation map of the frequencies measured in the evolution and detection periods, ω_1 and ω_2, respectively, and which parametrically depends on the mixing time t_m. In other words, the two-dimensional spectrum $S(\omega_1,\omega_2;t_m)$ represents the joint probability density of finding a benzene molecule in a certain orientation with respect to the external magnetic field, and thus a certain NMR frequency ω_1 during the evolution period t_1, and, after a time interval t_m later, finding the same benzene molecule with a NMR frequency ω_2 during the detection period t_2.

(48) Favre, D. E.; Schaefer, D. J.; Chmelka, B. F. Manuscript in preparation.

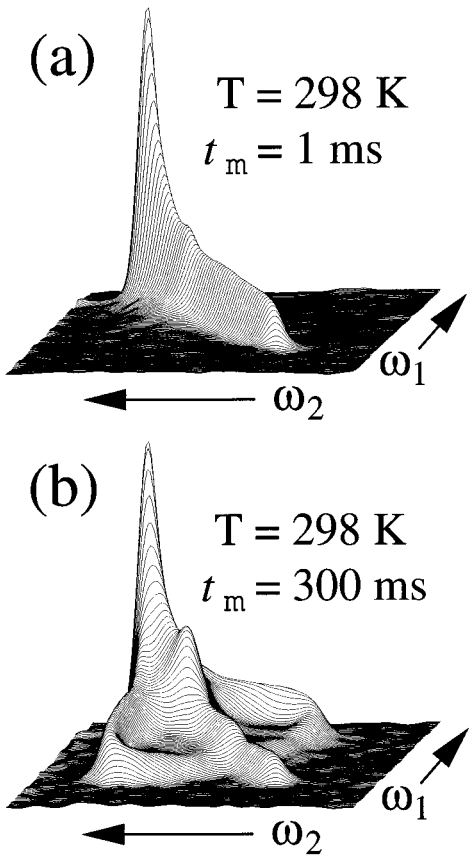

Figure 3. Experimental 2D exchange ^{13}C NMR spectra for benzene adsorbed in the supercages of Ca-LSX zeolite, acquired using the pulse sequence in Figure 2d. (a) $T = 298$ K, $t_m = 1$ ms, intensity along the diagonal ($\omega_1 = \omega_2$) reflects molecules in the same orientation with respect to the magnetic field $\mathbf{B}_0$ both before and after the mixing time t_m; exclusive intensity along the diagonal indicates that little or no exchange of benzene molecules occurs on this time scale among adsorption sites with different orientations. The central peak at 130 ppm results from benzene reorienting rapidly among either tetrahedrally arranged sites or isotropically, thereby averaging the chemical shift anisotropy to zero. A total of 160 scans for each t_1 increment was accumulated with a repetition time of 13 s, resulting in a total measuring time of 24 h. (b) $T = 298$ K, $t_m = 300$ ms; off-diagonal intensity in the 2D spectrum indicates molecular exchange during t_m among sites with different orientations. The elliptical features are consistent with a sizable fraction of benzene molecules reorienting among different well-defined environments situated $\beta = 109 \pm 3°$ with respect to one another. A total of 448 scans for each t_1 increment was accumulated with a repetition time of 13 s, resulting in a total measuring time of 66 h.

For example, Figure 3a displays the room-temperature 2D exchange ^{13}C NMR spectrum of benzene adsorbed on Ca-LSX zeolite showing an inhomogeneously broadened line shape that reflects an isotropic bulk distribution of benzene molecules. All spectral intensity is confined to the diagonal ($\omega_1 = \omega_2$) of the 2D plane, indicating that NMR frequencies have not changed during the course of the $t_m = 1$ ms mixing time, and consequently affirming that no detectable molecular reorientation has occurred among different adsorption sites on this time scale. The situation is considerably different in the spectrum of Figure 3b, which was acquired under identical conditions except for the use of a longer $t_m = 300$ ms mixing time. The spectrum in Figure 3b displays significant off-diagonal intensity in the form of an elliptical pattern and two straight lines that connect the singularity on the diagonal with the vertices of the ellipse. From the shape of the ellipse, the reorientation angle β between the relative orientations of an adsorbed molecule during t_1 and t_2 can be established directly according to[49]

$$|\tan \beta| = b/a \tag{3}$$

where a and b are the minor and major axes, respectively, of the elliptical pattern in the 2D exchange spectrum. For the present case of benzene adsorbed on Ca-LSX, a reorientation angle of 109° (or equivalently 71°, because reorientation angles of β and $(180° - \beta)$ cannot be distinguished on the basis of the NMR frequency alone, c.f. eq 1) is obtained, with an experimental uncertainty in the determination of about ±3°. These angles are consistent with the expected tetrahedral arrangements of benzene molecules adsorbed at Ca^{2+} cations at SII sites or adsorbed in 12-ring window sites within the supercages of the LSX structure.[7] Moreover, on closer inspection, the experimental 2D spectrum does not agree exactly with one simulated for a perfect tetrahedral jump process, with the deviations in the experimental line shape reflecting a narrow distribution of reorientation angles that will be analyzed quantitatively below. From a single 2D exchange experiment, detailed information about the geometry of the motional process can thus be determined.

The geometrical aspects of the site-hopping dynamics of benzene adsorbed on Ca-LSX can be probed in detail by exploiting the characteristic stimulated echoes of 2D exchange time-domain data, which are associated with inhomogeneously broadened spectra. The formation of a stimulated echo at a time $t_e \equiv t_2 = t_1$ after the start of the detection period becomes apparent from the 2D exchange time-domain signal, written for the special case of no exchange, $\omega_1 = \omega_2 = \omega$. The echo intensity, which depends parametrically on the mixing time t_m, can be written as[26]

$$\begin{aligned} s(t_1{=}t_e,t_2{=}t_e;t_m) &= \langle \cos(\omega t_e) \exp(i\omega t_e)\rangle \\ &= \langle {}^1/_2[\exp(-i\omega t_e) + \exp(i\omega t_e)] \exp(i\omega t_e)\rangle \\ &= {}^1/_2[1 + \langle \exp(i\omega 2t_e)\rangle] \end{aligned} \tag{4}$$

The "1" represents the normalized echo maximum, where independent of ω, all isochromats contribute equally to the signal. The exponential term represents the contribution of the so-called "virtual echo" with an unobservable maximum at $t_2 = -t_1$, that is, at a time t_1 before the beginning of the detection period at $t_2 = 0$. To analyze the geometry of a reorientation process, the normalized final-state stimulated-echo height $I_\infty(t_e)$, which is also called the final-state structure factor due to its analogy to the elastic incoherent structure factor (EISF) measured in quasielastic neutron scattering, must be considered as a function of t_e:[50]

$$I_\infty(t_e) = \frac{I(t_e;t_m \to \infty)}{I(t_e;t_m \to 0)} \tag{5}$$

where the normalized stimulated echo decay function $I(t_e;t_m)$ accounts for relaxation effects, which reduce by the factors $\exp(-t_e/T_2)$ and $\exp(-t_m/T_1)$ the stimulated-echo intensity $s(t_1{=}t_e,t_2{=}t_e;t_m)$ measured experimentally. This is achieved by multiplying the measured echo intensity by $s(0,0;\text{'0'})/s(0,0;t_m) = \exp(t_m/T_1)$ and $1/s(t_e,t_e;\text{'0'}) = \exp(t_e/T_2)/s_0$, which also eliminates the arbitrary intensity prefactor s_0 in the measured data to yield:[26]

(49) (a) Schmidt, C.; Wefing, S.; Blümich, B.; Spiess, H. W. *Chem. Phys. Lett.* **1986**, *130*, 84−90. (b) Schmidt, C.; Blümich, B.; Spiess, H. W. *J. Magn. Reson.* **1988**, *79*, 269−290.

(50) (a) Fujara, F.; Wefing, S.; Spiess, H. W. *J. Chem. Phys.* **1986**, *84*, 4579−4584. (b) Fujara, F.; Wefing, S.; Kuhs, W. F. *J. Chem. Phys.* **1988**, *88*, 6801−6809. (c) Fleischer, G.; Fujara, F. *NMR Basic Principles and Progress*; Springer Verlag: Berlin, 1994; Vol. 30, pp 161−207.

$$I(t_e;t_m) = s(t_e,t_e;t_m)\,\frac{1}{s(t_e,t_e;'0')}\,\frac{s(0,0;'0')}{s(0,0;t_m)} \qquad (6)$$

In practice, it is often sufficient to calculate $I_\infty(t_e)$ based on the ratio of the echo intensities for a mixing time $t_m \gg \tau_c$ and the echo intensity for the shortest accessible mixing time, usually $t_m = 1$ ms. In general, for an N-site jump with N equivalent sites[50]

$$\lim_{t_e\to\infty} I_\infty(t_e) = 1/N \qquad (7)$$

from which the number of distinct exchanging sites can be established. It is also important to realize that t_e acts as a "filter" in the experiment. For small values of t_e, only large-angle reorientations lead to changes in the NMR frequency that are sufficiently large to be detected as a reduction of the measured echo intensity. Thus, the larger the selected values of t_e, the more sensitive the experiment becomes toward small-angle motions.[50] The consequence of this is that small-angle reorientations within the mixing time will further reduce the experimentally measured echo heights, leading to deviations from the curve $I_\infty(t_e)$ corresponding to the large-angle reorientations, particularly for longer t_e values.

Whereas information on the geometrical aspects of benzene dynamics inside zeolite pore spaces can be obtained from a single 2D exchange spectrum, information on the time scale of the process requires that a set of 2D exchange spectra be acquired as a function of the mixing time t_m. The time scale can be quantified directly from the experimental spectra in several ways, most intuitively by computing the rise of the ratio $R^{2D}(t_m)$ of off-diagonal signal intensity to overall intensity from each individual spectrum. Alternatively, the motional time scale can be established by calculating the time-dependent orientational autocorrelation function $C_L(t_m)$:

$$C_L(t_m) = (2L+1)\,\langle P_L(\cos(\theta(t{=}0)))\,P_L(\cos(\theta(t{=}t_m)))\rangle \qquad (8)$$

where $L = 2$, 4, etc., denotes the order of the corresponding Legendre polynomial $P_L(\cos(\theta))$, directly from 2D exchange ($\eta = 0$) spectra according to

$$C_L(t_m) = (2L+1)\int\int \mathrm{d}\omega_1\,\mathrm{d}\omega_2\,S(\omega_1,\omega_2;t_m)\,p_L(\omega_1)\,p_L(\omega_2) \qquad (9)$$

with $p_L(\omega_i) = p_L(P_2(\cos(\theta_i)))$, that is, the higher order Legendre polynomials are expressed in terms of the second-order Legendre polynomials $\omega_i = P_2(\cos(\theta_i))$.[26] Complementary information to that obtained from the 2D exchange experiment is accessible by following the loss of correlation from the decrease of the echo intensity of the time-domain stimulated echo signal for selected values of the evolution time t_1 as a function of the mixing time.[50] The echo intensity is related to the diagonal fraction of the 2D exchange spectrum and can be used to probe the decrease of the spectral diagonal in favor of exchange intensity. Two-dimensional exchange ^{13}C NMR probes slow dynamics, typically in the correlation time window of 10^{-3} s $< t_m,\tau_c < 10^2$ s. If NMR frequencies change on a time scale faster than 1 ms, frequencies can no longer be considered constant during the evolution and detection periods and data analysis becomes more involved.[51] The upper limit for the mixing time t_m is established by spin−lattice relaxation, which causes the magnetization to decay to equilibrium with a time constant T_1 that is typically on the order of several seconds in ^{13}C NMR.

Exchange-Induced Sidebands (EIS). For the purpose of following the temperature dependence of the correlation times and obtaining an activation energy for the site-hopping motion of benzene adsorbed on Ca-LSX, acquisition of series of high-signal-to-noise-ratio 2D exchange spectra with varying mixing times at different temperatures is time consuming. This remains the case even if only the decay of the echo intensity in the time domain is followed for a few selected evolution times t_1, because to extract accurately the motional correlation time, the spin-lattice relaxation time T_1 should additionally be known at all relevant temperatures from independent measurements. To reduce the amount of time necessary to acquire spectra, while preserving direct and model-free extraction of the time scale of the hopping process under study, experimental techniques were consequently sought that yielded improved sensitivity over the static 2D exchange experiment. A one-dimensional MAS NMR experiment that is directly related to the static 2D exchange experiment and covers essentially the same correlation-time range in the slow motion limit has been designed by Yang et al.[33] The EIS experiment is briefly described below; for a more detailed description of the technique and the extraction of motional correlation times from EIS spectra, the reader is referred to ref 48.

High-resolution spectra of dilute spin-$^1/_2$ nuclei in condensed matter are obtained by using MAS NMR, that is, rapid spinning of a sample contained in a rotor inclined at an angle of 54.74° with respect to the external magnetic field $\mathbf{B}_0$, which results in a significant increase in sensitivity and spectral resolution compared to NMR on static (nonspinning) samples.[18b,22b,26,52] This is due to the averaging of anisotropic second-rank tensorial interactions, like chemical shift anisotropy (CSA), provided the sample rotation frequencies exceed the respective coupling strengths of the interaction. Slow sample spinning, that is, spinning at a frequency less than the CSA coupling strength, $\omega_R \le \delta$, however, breaks the inhomogeneously broadened line shape into sets of sideband patterns, which are separated according to their different isotropic chemical shifts. For comparison, Figure 4a shows a static CP NMR spectrum of benzene adsorbed on Ca-LSX, acquired at $T = 298$ K and using the pulse sequence in Figure 2a. The static CP spectrum is an axially symmetric powder pattern with the chemical shift tensor values of $\sigma_x = \sigma_y = 61 \pm 2$ ppm and $\sigma_z = -122 \pm 2$ ppm. Acquired under the same conditions, but with the benzene/Ca-LSX sample spinning with a rotation frequency of $\omega_R = 2\pi \times 2200$ Hz at the magic angle, Figure 4b shows the experimental CP MAS sideband spectrum. The centerband is at the isotropic chemical shift value for benzene, 130 ± 0.5 ppm, and would be the only observable line under fast spinning conditions, that is, at rotation frequencies exceeding the coupling strength of $\delta = 122 \pm 2$ ppm, which corresponds to $\delta = 5.5$ kHz in an external magnetic field strength of 4.2 Tesla. Thus, using low sample rotation frequencies, information about the anisotropy of the interaction is preserved in the intensities of the spinning sidebands, although at the expense of a decrease in angular resolution. Importantly, due to the confinement of the spectral intensity into a few narrow peaks, spectral sensitivity under MAS conditions is significantly enhanced compared to static NMR spectra.

In samples with an isotropic distribution of molecular orientations, the spinning sidebands can be suppressed through the use of the well-known TOSS technique,[40] the pulse sequence

(51) Kaufmann, S.; Wefing, S.; Schaefer, D.; Spiess, H. W. *J. Chem. Phys.* **1990**, *93*, 197−214.

(52) Stejskal, E. O.; Memory, J. D. *High Resolution NMR in the Solid State;* Oxford University Press: Oxford, 1994.

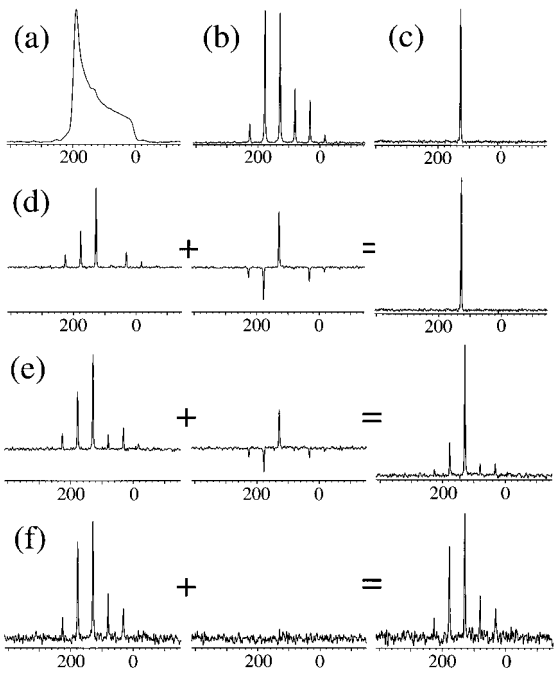

Figure 4. (a) Experimental static CP ^{13}C NMR spectrum of benzene adsorbed on Ca-LSX acquired at $T = 298$ K and using the pulse sequence in Figure 2a, showing an axially symmetric powder pattern with the chemical shift tensor values of $\sigma_x = \sigma_y = 61 \pm 2$ ppm and $\sigma_z = -122 \pm 2$ ppm, consistent with rapid rotation of benzene molecules about their 6-fold axes. A total of 384 scans has been averaged, using a repetition time of 15 s. (b) Experimental CP MAS ^{13}C NMR spectrum of benzene in Ca-LSX acquired at $T = 298$ K and a sample rotation frequency of $\omega_R = 2\pi \times 2200$ Hz, using the pulse sequence shown in Figure 2a. The centerband is at the isotropic chemical shift value for benzene, 130 ± 0.5 ppm, and spinning sidebands appear spaced apart by the sample rotation frequency. (c) Experimental TOSS ^{13}C NMR spectrum acquired under the same conditions as Figure 4b, but using the pulse sequence of Figure 2b. (d−f) Experimental EIS ^{13}C NMR spectra acquired with the pulse sequence shown in Figure 2c demonstrating the principle of the EIS experiment. For each mixing time, two spectra are acquired by varying the phase of the pulse before the mixing time; the two spectra are added to yield the final EIS spectrum. (d) $T = 298$ K, $t_m = 3$ ms, no exchange, the sideband intensities of the two spectra cancel, and a TOSS spectrum is obtained. (e) $t_m = 160$ ms, changes in the NMR frequencies due to molecular reorientation result in violation of the TOSS condition and the partial reappearance of spinning sidebands. (f) $t_m = 1600$ ms, full exchange (final state), the combined integrated area of the spinning sidebands reaches its maximum value of approximately 70% as compared to the conventional CP MAS spectrum shown in b. For all spectra (b−f) 32 scans were accumulated with a repetition time of 15 s.

for which is shown in Figure 2b. Application of the TOSS sequence produces 1D NMR spectra containing only peaks at the position of the isotropic chemical shift, as demonstrated in Figure 4c for the benzene/Ca-LSX system. The TOSS and exchange NMR experiments shown in Figures 2b and 2d, respectively, can be combined: incorporating TOSS in the preparation period of an exchange experiment allows the possibility of frequency changes during the subsequent mixing time that reintroduce sidebands in the 1D MAS spectrum acquired in the detection period. This combined experiment constitutes the EIS technique shown in Figure 2c, which allows much more rapid detection of molecular motions and the characterization of their related time scales than possible with the static 2D exchange NMR method.

In the EIS experiment, at the point where the acquisition begins in a standard TOSS measurement, the transverse ^{13}C magnetization is rotated into the z direction by a $\pi/2$-pulse, and a mixing time begins. The mixing period is allowed to last an integral number of rotor periods, during which frequency exchanges can occur that ultimately reintroduce spinning sidebands into the spectrum. At the end of the mixing period, the magnetization is returned to the transverse plane by another $\pi/2$-pulse for detection of the signal. Depending on the phase of the pulse at the beginning of the mixing period, either the sine or the cosine component of the transverse magnetization is selected for detection after the mixing period. Both components have to be measured and added to obtain pure absorption mode EIS spectra, see Figures 4d−f. Although this summation can be achieved in a single experiment by using the appropriate pulse phases and adding the time-domain signals, it is preferable to obtain the cosine and sine spectra in separate experiments and add the spectra afterward, thereby preserving the possibility to phase-correct them independently. In the absence of frequency changes due to, for example, molecular motions, the mixing period has no effect other than to allow spin−lattice relaxation to occur. Under these circumstances, the spectrum displays signals only at the isotropic chemical shifts, as shown in Figure 4d; the effect of magnetization created by spin−lattice relaxation is eliminated by proper phase cycling. In the presence of molecular motion, however, the delicate nonequilibrium state of the nuclear spins prepared by the TOSS sequence is perturbed during the mixing time and sidebands arise in the spectrum, as observed in Figure 4e,f.

Thus, the mere presence of spinning sidebands in a 1D EIS spectrum can provide evidence for molecular motion, as suppressed sidebands are restored as a result of molecular reorientation. The EIS experiment is conceptually closely related to the 2D exchange technique; in the case of slow exchange, it detects additional lines in a 1D measurement, a situation met otherwise only in multidimensional exchange NMR experiments.

Results and Discussion

The detailed geometry that underlies the site-hopping motions of benzene molecules among Ca^{2+} SII adsorption sites in Ca-LSX zeolite is revealed from the analyses of 2D exchange ^{13}C NMR spectra and time-domain data. From 1D EIS ^{13}C NMR spectra, the temperature dependence of the motional correlation times is extracted without recourse to a motional model, leading for the first time to direct measurements of activation energies for molecular transport events associated with hydrocarbon sorption in zeolites.

Geometry of Benzene Site-Hopping in Ca-LSX. Figure 5a shows a 2D exchange spectrum calculated for a jump motion between four identical tetrahedrally arranged sites and for $t_m \gg \tau_c$, so that the ratio of off-diagonal intensity to the overall intensity is 3:4. As an inset, the reorientation angle distribution $R(\beta;t_m)$ is shown, which in the case of $\eta = 0$ uniquely determines the 2D spectrum according to[26,53]

$$S(\omega_1,\omega_2;t_m) = \int_{0^\circ}^{90^\circ} d\beta\, R(\beta;t_m)\, S_\beta(\omega_1,\omega_2) \qquad (10)$$

This integral represents the sum of subspectra for each reorientation angle, $S_\beta(\omega_1,\omega_2)$, weighted by factors $R_f(\beta;t_m)$ for $0^\circ \le \beta \le 180^\circ$, which due to the equivalence of the spectra for β and $180^\circ - \beta$ must be restricted to $0^\circ \le \beta \le 90^\circ$:

$$R(\beta;t_m) = R_f(\beta;t_m) + R_f(180^\circ - \beta;t_m) \qquad (11)$$

(53) (a) Wefing, S.; Spiess, H. W. *J. Chem. Phys.* **1988**, *89*, 1219−1233. (b) Wefing, S.; Kaufmann, S.; Spiess, H. W. *J. Chem. Phys.* **1988**, *89*, 1234−1244.

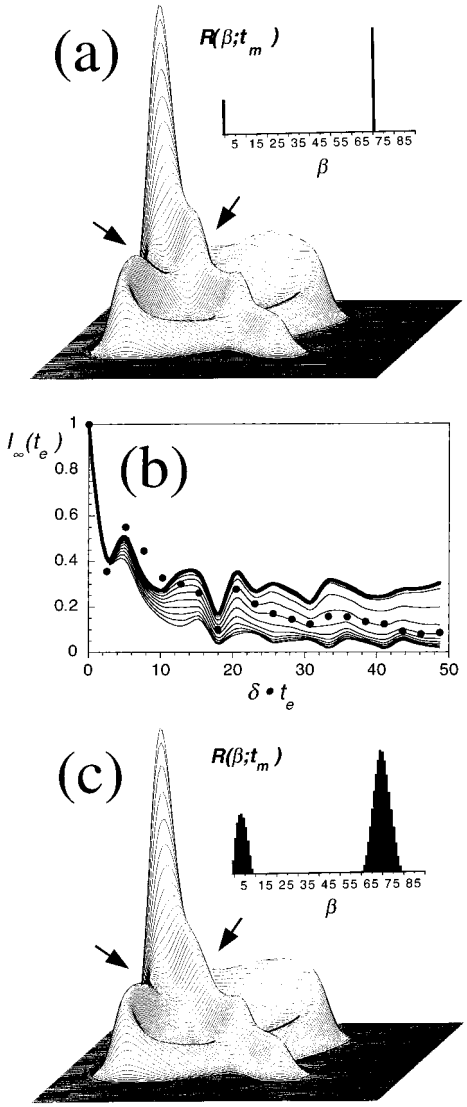

Figure 5. (a) Simulated 2D exchange spectrum calculated for a jump motion between four identical and exactly tetrahedrally arranged sites with $t_m \gg \tau_c$, i.e., conditions where full exchange prevails, resulting in a ratio of off-diagonal intensity to overall intensity of 3:4. The corresponding reorientation angle distribution $R(\beta;t_m)$ is shown as an inset. (b) The final-state structure factor $I_\infty(t_e)$ at $T = 298$ K is plotted together with simulated curves for exact tetrahedral jumps and jumps between the caps of cones with opening angles varying from 2° to 20° in 2° increments around the axis of a tetrahedron. For large values of t_e, the curve simulated for jumps between exact tetrahedral positions approaches the limit 0.25, as expected from eq 7. The experimentally observed values fall well below this value and follow the curves that were calculated for random jumps between cone caps, whose opening angles are estimated to be not less than 5° and not more than 15°.[54] (c) Simulated 2D exchange spectrum calculated for jumps between cone caps with 10° opening angles. The corresponding reorientation angle distribution $R(\beta;t_m)$ is shown as an inset. This simulated spectrum resembles more closely the experimental 2D exchange ^{13}C NMR spectrum of Figure 3b than the simulation for an exact tetrahedral jump process displayed in Figure 5a. The "wings" (see arrows) in the vicinity of the 90° singularity, which extend toward the vertices of the ellipse, are much better reproduced. A larger cone opening angle generates an even better fit in this region, but also leads to broadening of the diagonal portion of the spectrum to an extent not observed in the experiment and, furthermore, to pronounced deviations of $I_\infty(t_e)$, as observed from the curves shown in Figure 5b.

When this simulation is compared to the experimental spectrum in Figure 3b, acquired with a mixing time of $t_m = 300$ ms that is much longer than the correlation time $\tau_c = 35 \pm 7$ ms, it is seen that the major spectral features are shared, although the spectra differ in details. For example, differences in the intensity variations of the exchange singularities in the experimental and the simulated spectra are especially pronounced in the vicinity of the 90° singularity on the diagonal. This, together with the noticeably broader appearance of the diagonal portion of the experimental line shape, indicates that narrow distributions of benzene reorientation angles around the mean values of 0° and 109° (or equivalently 71°) are present in the experimental spectrum.

Examining such a distribution of reorientation angles further, time-domain stimulated echo data, and in particular the final-state structure factor $I_\infty(t_e)$, eq 5, provide sensitive means of gaining additional insight into the details of the geometry of benzene site-hopping in Ca-LSX. The function $I_\infty(t_e)$, that is, the normalized stimulated echo intensities as measured from the experimental 2D time-domain data at $T = 298$ K, is plotted in Figure 5b. Accompanying the experimental results are simulated curves for exact tetrahedral jumps and, as an example of a simple motional model leading to distributions of reorientation angles around the mean values of 0° and 109°, jumps between the caps of cones with different opening angles around the axis of a tetrahedron. For this model, the portion of the reorientation angle distribution that corresponds to the diagonal part of the 2D exchange spectrum is actually not centered around 0°, but around a value of half the opening angle of the cone, see Figure 5c. As expected from eq 7, for large values of t_e, the curve in Figure 5b that is simulated for jumps between exactly tetrahedral positions approaches the limiting value of 0.25. The experimentally observed and normalized (eq 6) values, however, fall well below this value, indicating the presence of effectively small-angle benzene molecular reorientations.

Moreover, the final-state structure factor data follow the curves in Figure 5b that were calculated for random jumps between cone caps, allowing the approximate width of such distributions to be established. Within experimental scatter, it can be estimated from the plot that the opening angle of each such cone is not less than 5° and not more than 15°, equivalent to angular deviations off the exact tetrahedral positions by about half the above values. The reorientation angle distributions centered around the two mean values are of almost Gaussian shape with their full-width-at-half-maximum (fwhm) given approximately by the cone opening angle. The estimate of the above angular limits is supported by the simulated 2D exchange spectrum displayed in Figure 5c, calculated for a cone opening angle of 10°, which resembles much more closely the essential features of the experimental spectrum in Figure 3b than does the simulated spectrum for an exact tetrahedral jump process displayed in Figure 5a. In the simulation of Figure 5c, the "wings" (see arrows) in the vicinity of the 90° singularity on the diagonal that extend toward the vertices of the ellipse are still not exactly reproduced and suggest the presence of a still wider distribution of reorientation angles. Use of larger cone opening angles, however, leads to pronounced deviations in the corresponding curves for $I_\infty(t_e)$, see Figure 5b, and also results in excessive broadening of the diagonal portion of the corresponding simulated 2D spectra to an extent not observed in the experimental spectrum. The application of other motional models[50b] more involved than simple jumps between cone caps results in a similar appearance of the curves for $I_\infty(t_e)$ and simulated 2D spectra. Consequently, the additional computational effort appears unwarranted in light of the already good agreement of the experimental data with the calculations for

(54) The final-state structure factor curve $I_\infty(t_e)$ is plotted as a function of the dimensionless variable δt_e, that is, the product of the echo time t_e and the chemical shift coupling strength δ (eq 1).

the simple model of jumps between cone caps. Higher resolution 2D exchange ^{13}C or ^{2}H NMR spectra, or $I_\infty(t_e)$ curves extending to even longer values of t_e, measured especially on ^{2}H with its larger anisotropy and increased angular resolution, would be necessary to help distinguish between different proposed geometries and motional models. Note that we have used the simple model of random jumps between cone caps solely to estimate the width of the distribution of reorientation angles, the existence of which is directly evident from the experimental data. This model creates a final-state reorientation angle distribution that reproduces the essential features of the experimental $I_\infty(t_e)$ data, although does not specify uniquely the temporal evolution of the molecular reorientation processes leading to this distribution.

In fact, recent molecular dynamics (MD) calculations by Auerbach[55] provide a plausible explanation for the occurrence of a distribution of jump angles that is also in accord with the reorientation angle distribution created by the simple motional model described above. For example, the MD results indicate that attractive interactions among benzene molecules occupying the same supercage lead to deviations from perfect tetrahedral geometry by angles that are in agreement with the ones deduced from the simulation of the NMR data above. The molecular dynamics calculations suggest two possibilities for the distribution of jump angles around 0°, both of which are consistent with the simple model proposed above. One explanation is that it results from benzene molecules hopping from one SII adsorption site to another by a jump angle in the vicinity of the tetrahedral angle and then back to the original site (or one oriented 180° from that of the starting position) through a slightly different angle, leading overall to a distribution around 0°. The second possibility is that slow small-angle reorientations are caused by adjustments in the positions of other benzene molecules made either as a response to another nearby benzene molecule hopping from one adsorption site to another or due to some other stochastic process that may be independent from the hopping between adsorption sites, although with a similar correlation time.

On the basis of the static structure factor $I_\infty(t_e)$ alone, the different origins of the effectively small-angle molecular reorientations cannot be distinguished. However, the distinction becomes clear upon comparing the temporal behavior of the echo intensity as a function of the mixing time for short ($t_e = 30\ \mu s$) and long ($t_e = 300\ \mu s$) values of t_e, i.e., the development of the reorientation angle distribution $R(\beta;t_m)$ with time. For the first model, the need for two hops in sequence means that the distribution around 0° would necessarily grow slower than the distribution around 109°, leading to a comparatively slower decay of the echo intensity for the longer values of t_e. For the second model, faster decay of the stimulated echo intensity would be observed when the small-angle motion is faster than the large-angle jump process, independent of whether the correlation time for the small-angle motion is related to the correlation time for the site-hopping motion or not.[50] The experimental data are only consistent with the latter model, showing faster correlation times with lengthening echo times t_e. Additional geometrical details of benzene site-hopping in Ca-LSX may be provided by recently developed 3D DIfference-COrrelated (DICO) NMR spectroscopy,[31] which is capable of detecting and quantifying slow small-angle fluctuations occurring together with large-angle jumps. Spin Alignment measurements,[50,56] essentially the ^{2}H NMR equivalent of the stimulated echo measurements described here, are also promising for a detailed study of the geometrical aspects of benzene orientation and reorientation inside the pores of a zeolite, because of the increased angular resolution provided by ^{2}H NMR.[57]

Correlation Times and Activation Energies of Benzene Site-Hopping. To investigate the temperature dependence of the motional correlation times for site-hopping of benzene adsorbed on Ca-LSX zeolite, as well as their dependence on the average bulk loading of benzene, EIS experiments were performed on Ca-LSX samples containing 0.5, 1, and 2 benzene molecules per supercage.[58]

From molecular dynamics simulations,[59] it is expected that four rate coefficients, k(SII→SII), k(SII→W), k(W→SII), and k(W→W) characterize the four distinct molecular hopping events of benzene molecules among SII cation and window (W) adsorption sites inside the pore space of the zeolite. The first three are indicated schematically in Figure 1b for a pair of adjacent LSX supercages. In the present investigation, we restrict consideration to an average bulk loading of up to 2 benzene molecules per supercage, for which it is anticipated that intercage benzene hops are much less frequent compared to intracage jumps and that no significant equilibrium population of benzene molecules in window sites exists; consequently, the rate coefficient k(W→W) is not indicated in Figure 1b. Support for a negligible amount of equilibrium adsorption of benzene in W sites is obtained from multiple-quantum (MQ) ^{1}H NMR studies of benzene distribution and spin coupling in Na-Y zeolite: for a bulk loading of 2 benzene molecules per supercage, no dipole−dipole coupling of ^{1}H spins on adsorbate species in adjacent cavities was observed up to the maximum MQ excitation time of 900 μs.[60] Even for benzene molecules adsorbed on substantially more weakly interacting Na^+ cation sites, appreciable window populations, which would serve to couple proton spins in adjacent cavities, are not expected for benzene concentration below ca. 3 molecules per supercage. Thus, the correlation times extracted from the experimental EIS data are expected to reflect predominantly the time scale for intracage site-hopping of benzene molecules among SII Ca^{2+} adsorption sites, k(SII→SII).

Correlation functions represent the simplest and most commonly used characterization of stochastic processes, such as benzene hopping between adsorption sites inside the cavities of a zeolite. Stochastic processes produce random fluctuations of nanoscopic variables, like the orientation of benzene with respect to the external magnetic field $\mathbf{B}_0$, that can be described by a characteristic time constant, the correlation time τ_c. As indicated above, the simplest correlation function that can be probed with NMR is the time-dependent second-order orientational autocorrelation function $C_2(t_m)$, which can be calculated directly from 2D exchange ($\eta = 0$) spectra:

$$C_2(t_m) = \frac{\langle P_2(\cos(\theta(t=0)))\, P_2(\cos(\theta(t=t_m)))\rangle}{\langle P_2{}^2(\cos(\theta(t=0)))\rangle} = \frac{\langle \omega(0)\, \omega(t_m)\rangle}{\langle \omega^2(0)\rangle} = 5 \int\int d\omega_1\, d\omega_2\, S(\omega_1,\omega_2;t_m)\, \omega_1\omega_2 \qquad (12)$$

(55) Saravanan, C.; Auerbach, S. M. Submitted to *J. Chem. Phys.*
(56) Spiess, H. W. *J. Chem. Phys.* **1980**, *72*, 6755−6762.
(57) Isfort, O.; Fujara, F. To be published.
(58) All variable-temperature and benzene-loading experiments were performed on Ca-LSX material synthesized and characterized in our laboratory. Equivalence in the geometrical aspects of benzene reorientation for this material and that used in the 2D investigation described in ref 32 was confirmed by 2D exchange ^{13}C NMR, which yielded a spectrum indistinguishable from that shown in Figure 3b.
(59) Auerbach, S. M. *J. Chem. Phys.* **1997**, *106*, 7810−7815.

Each correlation function $C_L(t_m)$ of eq 8 can also be calculated from the reorientation angle distribution $R(\beta;t_m)$ according to

$$C_L(t_m) = \langle P_L(\cos(\beta;t_m))\rangle = \int_{0°}^{90°} d\beta\, R(\beta;t_m)\, P_L(\cos(\beta)) \tag{13}$$

Equation 13 allows for straightforward calculations of $C_L(t_m)$ based solely on the reorientation angle distribution introduced above.

In the following, the definitions of the various rate coefficients and time constants used in conjunction with the description of stochastic processes in terms of correlation functions will be briefly summarized. As an example, for the simple case of a N-site jump motion with the jump rate k_{hop} from one site to another, the second-order orientational correlation function decays exponentially to a plateau value $\lim_{t\to\infty} C_2(t;\beta)$, which depends on the reorientation angle β (for example, $\lim_{t\to\infty} C_2(t;\beta = 109.5°) = 0$):

$$C_2(t_m) = (1 - \lim_{t\to\infty} C_2(t;\beta)) \exp(-\lambda t_m) + \lim_{t\to\infty} C_2(t;\beta) \tag{14}$$

with the relaxation rate $\lambda = Nk_{hop}$. Using the definition of an autocorrelation time τ_c:[61]

$$\tau_c = \int_0^\infty dt_m \frac{\langle\omega(0)\,\omega(t_m)\rangle - \lim_{t\to\infty}\langle\omega(0)\,\omega(t)\rangle}{\langle\omega^2(0)\rangle - \lim_{t\to\infty}\langle\omega(0)\,\omega(t)\rangle}$$

$$= \int_0^\infty dt_m \frac{C_2(t_m) - \lim_{t\to\infty} C_2(t)}{(1 - \lim_{t\to\infty} C_2(t;\beta))}$$

$$= \int_0^\infty dt_m \exp(-\lambda t_m) = \frac{1}{Nk_{hop}} \tag{15}$$

If one defines a microscopic rate coefficient k_{mic} as the overall rate to leave a single site, $k_{mic} = (N - 1)k_{hop}$, the relation between the correlation time τ_c, and k_{mic} is

$$\tau_c = \frac{1}{Nk_{hop}} = \frac{N-1}{Nk_{mic}} \tag{16}$$

Frequently, the time scale is characterized by the inverse of the microscopic rate coefficient, called the residence time, τ_{res}, at a given site:

$$\tau_{res} = \frac{1}{k_{mic}} = \frac{1}{(N-1)k_{hop}} \tag{17}$$

Furthermore, for a N-site jump motion, the correlation time τ_c can be extracted directly from the mixing-time-dependent function $R^{EIS}(t_m)$, which is the ratio of the combined integrated area of all sidebands to the overall integrated area of all peaks in the EIS spectrum, according to[48]

$$R^{EIS}(t_m) = R_{fe}(1 - \exp(-t_m/\tau_c)) \tag{18}$$

where R_{fe} corresponds to the ratio $R^{EIS}(t_m)$ in the limit of full exchange, that is, $t_m \gg \tau_c$. Equation 18 is used in this investigation to obtain fits to the experimentally determined values of $R^{EIS}(t_m)$, with the only unknown being the correlation time τ_c, as R_{fe} is measured experimentally. Over the 200−338 K temperature range and benzene/Ca-LSX adsorbate loadings investigated, no significant deviations of $R^{EIS}(t_m)$ from monoexponential behavior were observed. If necessary, eq 18 can be generalized without difficulty to allow bi- or nonexponential fits to the experimental data. Equation 18 is analogous to the expression obtained for the ratio of off-diagonal-to-overall integrated signal areas of static 2D exchange spectra. They differ, however, in one regard. In the expression for 2D exchange spectroscopy on a nonspinning sample, the factor R_{fe} is directly related to the number of equivalent sites, $R_{fe} = (N - 1)/N$, and thus to the geometry of the motional process. However, in the case of the EIS experiment, R_{fe} is a complicated function of the MAS rotation frequency, $R_{fe} = R_{fe}(\omega_R)$,[48] which precludes its use for establishing the number of exchanging sites.

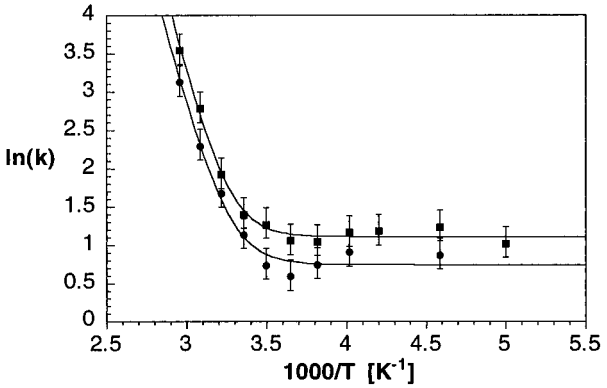

Figure 6. Temperature dependence of the rate coefficients for average bulk loadings of 0.5 (circles) and 2 (squares) benzene molecules per supercage in Ca-LSX zeolite, as extracted directly from exchange-induced-sidebands ^{13}C NMR spectra. In the Arrhenius plots, two different processes can clearly be identified for both loadings. The high-temperature process is attributed to site-hopping of benzene molecules among SII Ca^{2+} sites in the supercages of the faujasite LSX structure; the low-temperature process is identified as proton-driven ^{13}C spin diffusion among adjacent benzene molecules. The solid lines in the diagrams represent fits of $\ln[k_0 \exp(-E_a/RT) + 1/\tau_{SD}]$ to the values $\ln(k) = \ln(1/\tau_c)$, with τ_c obtained from an exponential fit to $R^{EIS}(t_m)$ of the experimental EIS spectra. The values for E_a and k_0 obtained for the different loadings are compiled in Table 3.

Both, the 2D exchange and the 1D EIS results therefore yield model-independent measurements of the motional correlation times τ_c associated with slow molecular reorientation processes. Such correlation times, as for example obtained from a fit to the ratio $R^{EIS}(t_m)$ (eq 18), can be equivalently expressed as model-independent rate coefficients k according to the simple relation $k = 1/\tau_c$; k is then identical to the relaxation rate λ introduced in eq 14, using the relation:

$$R^{EIS}(t_m)/R_{fe} = (1 - C_2(t_m))/(1 - \lim_{t\to\infty} C_2(t;\beta)) \tag{19}$$

In light of the 4-site jump motion of benzene molecules among Ca^{2+} SII cations in Ca-LSX, the rate coefficient k is equal to $4k_{hop}$, with k_{hop} being the jump rate from one site to another, or equivalently, $4k_{mic}/3$, where k_{mic} is the microscopic hopping rate for a molecule leaving one site. The use of rate coefficients as opposed to correlation times gives the resulting Arrhenius diagrams a more familiar appearance. Nevertheless, a *model-independent* correlation time is the important primary result obtained from the experimental exchange NMR data. Conversion of the correlation times into rate coefficients, such as k_{hop} or k_{mic} above, unnecessarily obscures the model independence of the analysis, and it is for this reason that we henceforth use $k = 1/\tau_c$ and drop all (model-related) factors.

(60) Pearson, J. G.; Chmelka, B. F.; Shykind, D. N.; Pines, A. *J. Phys. Chem.* **1992**, *96*, 8517−8522.

(61) Oppenheim, I.; Shuler, K. E.; Weiss, G. H. *Stochastic Processes in Chemical Physics: The Master Equation;* MIT Press: Cambridge, 1977.

In Figure 6, the temperature dependence of the rate coefficients k extracted from the EIS spectra over a temperature range from 200 to 338 K are presented as Arrhenius diagrams for two samples containing average bulk loadings of 0.5 and 2 adsorbed benzene molecules per Ca-LSX supercage. Measurements have also been carried out for an average bulk loading of 1 benzene molecule per Ca-LSX supercage, with the rate coefficients lying between those presented for the lower and higher benzene concentrations; these intermediate data have been omitted for clarity. As shown in Figure 6, the results for each of the samples reflect the existence of two distinct processes: a nonactivated one below approximately 273 K, for which the rate coefficients do not vary with temperature, and an activated process above 273 K, which displays a strong Arrhenius temperature dependence. Furthermore, rate coefficients in both temperature regimes tend to increase with an increase in average bulk loading.

The rather unusual observation of temperature-independent rate coefficients in the low-temperature region is caused by the process of spin diffusion,[62] that is, magnetization transfer mediated by $^{13}C-^{13}C$ dipolar couplings, among benzene molecules that may or may not reorient to different adsorption sites on the time scale of the NMR measurement. The sensitive r^{-6} dependence of the spin-diffusion rate constant on the internuclear distance r separating dipole−dipole coupled nuclei has allowed spin diffusion to be used in other systems to probe material structural heterogeneities especially on mesoscopic length scales, such as spatial proximities and sizes of domains in polymer blends.[26,63] However, for the present case and others where the time scale of reorientational dynamics is the primary objective, the occurrence of spin diffusion is complicating and undesirable. This is because spin diffusion creates off-diagonal intensity in 2D exchange spectra or leads to the reappearance of spinning sidebands in EIS spectra in much the same way as does molecular reorientation. As a result, intensity patterns in exchange NMR spectra may have contributions from both processes, in this case the hopping of benzene molecules among discrete adsorption sites and magnetization transfer via $^{13}C-^{13}C$ dipolar couplings among both reorienting and nonreorienting benzene molecules. Thus, the presence of spin diffusion complicates the extraction of the motional component of the correlation times τ_c obtained directly from the experimental EIS spectra (see eq 18) acquired in the high-temperature region. In each spectrum, the exchange intensity contribution resulting from the spin diffusion process must be either eliminated or properly accounted for. As will be shown below, all efforts to eliminate or sufficiently suppress the spin diffusion process for benzene adsorbed on Ca-LSX have proven ineffective. Consequently, accurate measurement of the rate constant associated with the spin diffusion process at low temperatures is required, so that the rate coefficients measured in the high-temperature regime can be accurately corrected. Assuming that spin diffusion and the site-hopping motion of benzene molecules are independent processes, the overall correlation times τ_c, as obtained directly from the experimental EIS spectra, can be separated into the respective contributions according to

$$\frac{1}{\tau_c} = \frac{1}{\tau_M} + \frac{1}{\tau_{SD}} \Leftrightarrow \frac{1}{\tau_M} = \frac{1}{\tau_c} - \frac{1}{\tau_{SD}} \tag{20}$$

where τ_M stands for the correlation time of the dynamic molecular site-hopping process and τ_{SD} for the spin-diffusion correlation time. Doing so provides precise and accurate determination of the motional correlation times for the benzene site-hopping dynamics in Ca-LSX, from which the sought-after activation energies for these molecular transport events can be readily established.

Low-Temperature Regime: Spin Diffusion. The exchange NMR spectra from which Figure 6 is compiled are dominated at low temperatures by spin diffusion among benzene molecules that are ^{13}C-enriched in a single site. Furthermore, decreasing the average bulk loading from 2 benzene molecules per supercage to 0.5 benzene molecules per supercage does not effectively suppress the spin diffusion process, as seen clearly in Figure 6, which displays the characteristic rate-coefficient plateau at the lower adsorbate concentration as well. Another means of reducing the spin diffusion efficiency is to use benzene with ^{13}C in natural abundance (1.1 atom %), which diminishes the probability of two ^{13}C nuclei being near each other, thus rendering $^{13}C-^{13}C$ dipole−dipole coupling less efficient. A series of EIS experiments on Ca-LSX with an average bulk loading of 2 non-^{13}C-enriched benzene molecules per supercage was performed at $T = 238$ K; no indication of sideband intensity was observed up to a mixing time of 3.44 s. This observation demonstrates that molecular reorientation dynamics do not occur to a measurable extent at $T = 238$ K on the order of seconds. This in turn establishes spin diffusion as the dominant process in the low-temperature regime, where on this time scale spinning sidebands are almost fully restored for Ca-LSX samples loaded with 99% ^{13}C-enriched benzene. While spin diffusion efficiency is reduced in the benzene/Ca-LSX system by using ^{13}C in natural abundance, its use unfortunately leads to significantly reduced signal sensitivity as well. This results in prohibitively long measuring times to obtain reasonable quality 1D EIS spectra, so that exchange NMR experiments relying on naturally abundant ^{13}C in benzene/Ca-LSX samples are infeasible, at least for routine measurements. A compromise, in which single-site ^{13}C-enriched benzene was diluted 1:9 with benzene with ^{13}C in natural abundance, proved similarly insufficient to suppress spin diffusion on the time scale needed (∼1 s). This exhausts the easily accessible options for eliminating magnetization transfer that occurs because of dipolar couplings, which thus require more aggressive efforts to suppress in the benzene/Ca-LSX system.

In general, spin diffusion occurs because of simultaneous energy conserving spin flips (flip−flops) involving pairs of dipolar-coupled nuclei that cause magnetization to be transported through a sample.[62] In the case of two spins having different resonance frequencies, such as those in benzene molecules having different orientations at different Ca-LSX adsorption sites (Figure 1b) in high magnetic fields, this flip−flop process is forbidden unless there are external contributions to the energy balance. In so-called "proton-driven" spin diffusion, the interaction of the ^{13}C nuclei with the proton reservoir compensates for the local frequency mismatch caused by different orientations of adsorbed benzene molecules with respect to the external magnetic field $\mathbf{B}_0$, allowing mutual spin flips to occur. Under such circumstances, suppressing $^{1}H-^{13}C$ couplings by high-power proton decoupling will suppress the $^{13}C-^{13}C$ magnetization transfer.[64] This was exploited by performing

(62) (a) Meier, B. H. In *Advances in Magnetic and Optical Resonance;* Warren, W.S., Ed.; Academic Press: New York, 1994; Vol. 18, pp 1−116. (b) Suter, D.; Ernst, R. R. *Phys. Rev. B* **1985**, *32*, 5608−5627. (c) Vanderhart, D. L. *J. Magn. Reson.* **1987**, *72*, 13−47. (d) Kubo, A.; McDowell, C. A. *J. Chem. Phys.* **1988**, *89*, 63−70. (e) Henrichs, P. M.; Linder, M.; Hewitt, J. M. *J. Chem. Phys.* **1986**, *85*, 7077−7086. (f) Tycko, R.; Dabbagh, G. *Isr. J. Chem.* **1992**, *32*, 179−184. (g) Diezemann, G. *J. Chem. Phys*. **1995**, *103*, 6368−6384.

(63) (a) Clauss, J.; Schmidt-Rohr, K.; Spiess, H. W. *Acta Polym.* **1993**, *44*, 1−17. (b) Vanderhart, D. L. *Makromol. Chem., Macromol. Symp.* **1990**, *34*, 125−159. (c) Wang, J. *J. Chem. Phys.* **1996**, *104*, 4850−4858. (d) Linder, M.; Henrichs, P. M.; Hewitt, J. M.; Massa, D. J. *J. Chem. Phys.* **1985**, *82*, 1585−1598

static 2D exchange experiments with high-power $^1H-^{13}C$ decoupling continued during the mixing time to confirm unambiguously that spin diffusion is the dominant process at low temperatures (<273 K). Although not shown here, a strong reduction in off-diagonal exchange intensity was observed in a 2D exchange spectrum acquired at $T = 173$ K with $t_m = 300$ ms and with high-power proton decoupling applied during the mixing time, compared to a 2D exchange spectrum acquired without proton decoupling during the mixing time under otherwise identical conditions.[65] The significant reduction of the off-diagonal signal proves conclusively that the exchange intensity at low temperatures is caused almost entirely by spin diffusion and not by dynamic reorientation of benzene molecules among adsorption sites. Although the power level for the heteronuclear decoupling can be somewhat reduced during the mixing time from the level usually applied during acquisition of the NMR signal, the severity of this method renders it unsuitable for routine applications and longer mixing times due to the inherent danger of damaging the NMR equipment. Moreover, under slow MAS conditions, suppressing the proton-driven spin diffusion by applying proton decoupling during the mixing time of an EIS experiment can even result in increased spin diffusion efficiency, when conditions of rotational resonance are met.[66] Under these circumstances, where the frequency difference between two ^{13}C spins is matched by the rotation frequency of the MAS sample rotor, so-called "rotor-driven" spin diffusion prevails, contributing additional complexity to the subsequent analysis.

Thus, the infeasibility of eliminating the spin diffusion process requires that the spin-diffusion rate constants be accurately measured at low temperatures as the only means to correct the rate coefficients obtained at high temperatures where benzene reorientation dynamics prevail. The correction applied necessarily assumes that the spin diffusion process is not influenced by the site-hopping motion of the benzene molecules in the high-temperature regime, or, in other words, that the two processes are uncoupled, see eq 20. The spin-diffusion rate constant is thus presumed to remain constant with temperature. In certain instances, coupling of the spin diffusion and dynamic processes has been observed, which can produce higher spin diffusion rates at higher temperatures.[62g,67] However, this is not expected to be a factor in the present investigation, as the rate coefficients associated with benzene site-hopping are generally small enough that the reorientation dynamics remain uncoupled to spin diffusion except perhaps for the fastest rate coefficients reported here. Even then, coupling of the two processes will have no influence on the activation energy measured, because the spin diffusion process will necessarily display the same apparent activation energy as the motional process that causes its temperature dependence.[66]

To legitimize the assumption of temperature-independent spin diffusion rates in the present investigation, 2D exchange spectra with high-power proton decoupling during the mixing time were acquired in the high-temperature regime and for mixing times on the order of the motional correlation time. No difference in the exchange intensity was found when these spectra were compared to spectra obtained without such proton decoupling applied during the mixing time, establishing at least that the spin-diffusion rate constants did not change significantly (if at all) over the temperature range investigated.[65] The temperature-independent correlation times $\tau_c = \tau_{SD} = 1/k_{SD}$ established for the $^{13}C-^{13}C$ spin diffusion process for different loadings of single-site ^{13}C-enriched benzene adsorbed on Ca-LSX zeolite are given in Table 1, as extracted from EIS experiments conducted at temperatures from 200 to 274 K.

Table 1. Correlation Times and Rate Coefficients for Spin Diffusion Extracted from Experimental EIS ^{13}C NMR Spectra Acquired in the Low-Temperature Regime (200−274 K) for Average Bulk Loadings of 0.5, 1, and 2 Benzene Molecules per Supercage Adsorbed on Ca-LSX[a]

	0.5 benzene/ supercage	1 benzene/ supercage	2 benzene/ supercage
τ_{SD}, s	0.45 ± 0.1	0.37 ± 0.1	0.35 ± 0.1
$k_{SD} = 1/\tau_{SD}$, s^{-1}	2.22 ± 0.5	2.70 ± 0.8	2.86 ± 0.9

[a] Adsorbed benzene molecules were 99% ^{13}C-enriched in a single site to increase signal sensitivity. The correlation time is obtained from a fit of eq 18 to the experimental EIS data; the inverse of the correlation time represents a model-independent rate coefficient.[68]

Table 2. Comparison of Correlation Times at Different Temperatures as Extracted from Measurements of Benzene Adsorbed on Ca-LSX for an Average Bulk Loading of 2 Benzene Molecules per Supercage[a]

T, K	τ_c, as measured, ^{13}C, single site, s	$\tau_M = (\tau_c^{-1} - \tau_{SD}^{-1})^{-1}$, ^{13}C, single site, s	$\tau_c = \tau_M$, as measured, ^{13}C, nat. abund., s
324	0.07 ± 0.01	0.08 ± 0.02	0.05 ± 0.01
298	0.26 ± 0.02	0.8 ± 0.2	0.7 ± 0.1

[a] One sample contained ^{13}C-enriched benzene and the other sample used benzene with ^{13}C in natural abundance. The second and fourth columns contain the correlation times τ_c, as obtained directly from fits of eq 18 to the data. The third column lists the motional correlation time τ_M associated with the hopping of benzene molecules between SII cations, after the correction for spin diffusion (eq 20) was applied to the results from the ^{13}C-enriched sample.

Correcting the rate coefficients in the high-temperature regime by applying eq 20 enables activation energies for the high-temperature process(es) to be accurately determined, the values of which are otherwise too low and incorrect. Further experimental verification that the two processes are indeed independent was obtained by comparing the motional rate coefficients obtained for two samples with loadings of 2 benzene molecules per supercage, one using single-site ^{13}C-enriched benzene and the other using benzene with ^{13}C in natural abundance. The results of this comparison are compiled in Table 2. At both $T = 298$ K and $T = 324$ K, the motional correlation times τ_M obtained with single-site ^{13}C-enriched benzene after correction for the spin-diffusion process, $\tau_{SD} = 0.35$ s (from Table 1), are the same within experimental uncertainty as the values obtained with ^{13}C in natural abundance. The comparison in Table 2, thus, again supports the temperature independence of the spin-diffusion rate constant over the entire temperature range from 200 to 338 K.

Because spin diffusion is mediated by dipolar couplings that are highly dependent on the distance between the two coupled nuclei (dipolar coupling strength $\sim r^{-3}$, spin-diffusion rate constant $\sim r^{-6}$), information about the average distance of two benzene molecules in the supercages of Ca-LSX is in principle obtainable from the data in Table 1. Consistently, an increase

(64) Limbach, H.-H.; Wehrle, B.; Schlabach, M.; Kendrick, R.; Yannoni, C. S. *J. Magn. Reson.* **1988**, *77*, 84−100.

(65) Favre, D. E. Ph.D. Dissertation, University of California, Santa Barbara, manuscript in preparation.

(66) (a) Gan, Z.; Ernst, R. R. *Chem. Phys. Lett.* **1996**, *253*, 13−19. (b) Colombo, M. G.; Meier, B. H.; Ernst, R. R. *Chem. Phys. Lett.* **1988**, *146*, 189−196. (c) Challoner, R.; Kümmerlen, J.; McDowell, C. A. *Mol. Phys.* **1994**, *83*, 687−700. (d) Maas, W. E. J. R.; Veeman, W. S. *Chem. Phys. Lett.* **1988**, *149*, 170−174. (e) Kubo, A.; McDowell, C. A. *J. Chem. Soc., Faraday Trans. 1* **1988**, *84*, 3713−3730.

(67) (a) Müller, A.; Haeberlen, U. *Chem. Phys. Lett.* **1996**, *248*, 249−254. (b) Müller, A.; Zimmermann, H.; Haeberlen, U. *J. Magn. Reson.* **1997**, *126*, 66−78.

(68) Note that the symmetric error range of the correlation time transfers into an unsymmetric error range for the rate coefficient; for the sake of simplicity, averages of the high- and low-end uncertainty values are tabulated.

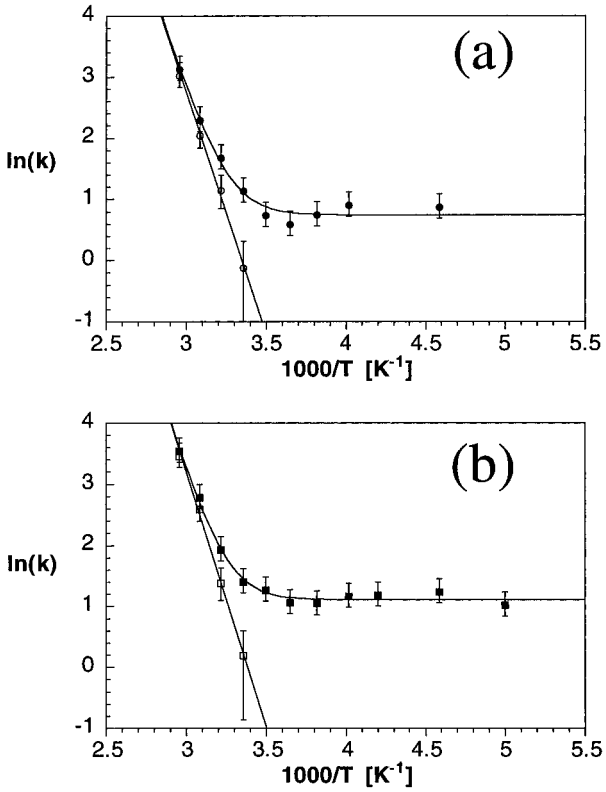

Figure 7. Arrhenius diagrams of rate coefficients for site-hopping of benzene molecules adsorbed on Ca-LSX at two different bulk loadings, comparing the rate coefficients as determined from the experimental EIS spectra, $k = 1/\tau_c$ (filled symbols, see Figure 6), and after correction for spin diffusion, $k = 1/\tau_M$ (open symbols). (a) Average bulk loading of 0.5 benzene molecules per Ca-LSX supercage. The apparent activation energy for the molecular hopping process is found to be $E_a = 65 \pm 6$ kJ mol^{-1}; the preexponential factor is determined to be 5×10^{11} s^{-1}. (b) Average bulk loading of two benzene molecules per Ca-LSX supercage. At this higher loading the apparent activation energy is found to be $E_a = 68 \pm 7$ kJ mol^{-1}; the preexponential factors is determined to be 1×10^{12} s^{-1}.

of the spin-diffusion rate constant is observed as the average bulk loading is increased. This agrees with the expected higher probability of having an increased number of supercages with more than one benzene molecule at higher loadings, consistent with a reduction of the mean separation distance between coadsorbed benzene molecules. However, the observed loading dependence of the spin-diffusion rate constant is relatively weak, in spite of the sensitive r^{-6} dependence, so that the overall differences in benzene distribution on the molecular length scale appear to be minor. More detailed information, however, requires *a priori* knowledge of the spin-diffusion rate constant for a given distance between two coupled ^{13}C nuclei. Theoretical calculations of the spin-diffusion rate constant requires knowledge of parameters, like the width of the zero-quantum line shape or the magnitude of the overlap of single-quantum line shapes used to estimate the breadth of the zero-quantum line shape, which are difficult to measure or to estimate precisely for the benzene/Ca-LSX system.[69] A few experimental determinations of spin-diffusion rate constants between two coupled ^{13}C spins exist, although their direct applicability to the benzene/Ca-LSX system is questionable in view of differences in the strengths of the dipolar couplings and dynamical behaviors present in the various systems.[63d,66a,69] Nevertheless, in comparison to the cited spin-diffusion rate constants, the values reported in this investigation appear reasonable for the ~0.5 nm distances separating benzene molecules adsorbed on SII cations in the supercages of Ca-LSX zeolite.

(69) Robyr, P.; Tomaselli, M.; Straka, J.; Grob-Pisano, C.; Suter, U. W.; Meier, B. H.; Ernst, R. R. *Mol. Phys.* **1995**, *84*, 995−1020.

Table 3. Summary of Apparent Arrhenius Activation Energies, E_a, and Preexponential Factors, k_0, for Benzene Molecules Hopping between Ca^{2+} SII Adsorption sites in Ca-LSX Zeolite in Samples with Average Bulk Loadings of 0.5, 1, and 2 Benzene Molecules per Supercage

	0.5 benzene/ supercage	1 benzene/ supercage	2 benzene/ supercage
E_a, kJ mol^{-1}	65 ± 6	65 ± 6	68 ± 7
k_0, s^{-1} ($\pm$ 1 decade)	5×10^{11}	1×10^{12}	1×10^{12}

High-Temperature Regime: Spin Diffusion and Molecular Dynamics. Apparent Arrhenius activation energies for benzene site-hopping between Ca^{2+} adsorption sites in Ca-LSX are obtained from the temperature dependence of the rate coefficients in the high-temperature regime (>273 K, see Figures 6 and 7). The overall rate coefficients are extracted from a fit of eq 18 to the experimental EIS spectra intensities and must be corrected, as discussed above, by applying eq 20 to account for the effects of spin diffusion. Two possibilities exist to obtain the corrected activation energies; both are equivalent and take into account that spin diffusion and the four-site jump motion of benzene molecules among adsorption sites observed at higher temperatures are independent processes. First, assuming an Arrhenius-type temperature dependence for the rate coefficients in the high-temperature regime and with a temperature-independent rate constant for the spin diffusion process, a fit of $\ln[k_0 \exp(-E_a/RT) + k_{SD}]$ to the values $\ln(k) = \ln(1/\tau_c)$ can be performed, using k_0 and E_a as adjustable parameters. These fits are the solid lines included in Figure 6, with the corresponding values for the apparent Arrhenius activation energy E_a and the Arrhenius preexponential factor k_0 compiled in Table 3. The spin-diffusion rate constants $k_{SD} = 1/\tau_{SD}$, as determined previously from analyses in the low-temperature regime, are summarized in Table 1. The values of the preexponential factors k_0, which are nearly identical for the three average bulk loadings of 0.5, 1, and 2 benzene molecules per supercage, are consistent with values for elementary adsorption processes;[17d] their uncertainty of about $\pm$1 decade arises mostly from the extrapolation of measurements in a narrow temperature range of about 60 K, and is increased due to the experimental uncertainties in the determination of spin-diffusion rate constants. The apparent Arrhenius activation energies E_a for the three different benzene concentrations are also identical within experimental scatter; the apparent increase in the rate coefficients with loading is not reflected in the observed activation energies.

The degree to which each rate $k = 1/\tau_c$ requires correction for the parallel spin diffusion process is more easily seen if $k = 1/\tau_M$ is plotted and compared to $k = 1/\tau_c$ (as in Figure 6), with τ_M being the motional correlation time obtained by applying eq 20 to the values of τ_c extracted from the fits to eq 18. From the temperature dependence of the motional correlation times τ_M obtained, the apparent Arrhenius activation energies can then be computed. Part a and b of Figure 7 show Arrhenius plots for the two bulk loadings of 0.5 and 2 benzene molecules per Ca-LSX supercage, in which the rate coefficients obtained from fits to the exchange intensity ratios $R^{EIS}(t_m)$ of the experimental EIS spectra are accompanied by rate coefficients that have been corrected for temperature-independent spin-diffusion contributions. The error bars in Figure 7a,b take the variation of the uncorrected rates into account, as well as the variation in the measured spin-diffusion rate constants. One can see that the corrections made to the correlation times τ_c can be quite

significant, but only in the transition between the high- and low-temperature regimes. It is mostly the uncertainty of the rate coefficients in this transition range which yields the uncertainty in the determination of the Arrhenius prefactor k_0.

Moreover, for the 200−338 K temperature range investigated and average bulk loadings of 0.5−2 benzene molecules per supercage, no significant deviation from a monoexponential correlation function was observed for the exchange intensity ratio $R^{EIS}(t_m)$. Alhough at least two processes contribute to the EIS spectra, these results affirm that spin diffusion is the dominant contribution to the exchange intensity in the low-temperature regime, whereas in the high-temperature regime the site-hopping motion dominates. Solely monoexponential behavior in the high-temperature regime furthermore reflects either the similarity of the intra- and intercage rate coefficients or a negligible number of benzene molecules undergoing intercage-hopping processes (within the sensitivity of the measurements). These two possibilities are distinguished from each other by the different relative magnitudes of the motional correlation times characterizing the intracage and intercage dynamics. On the basis of computer simulations of the dynamics of benzene molecules adsorbed on closely related Na-X and Na-Y zeolites,[17b−d,23b] intracage adsorbate exchange with the rate coefficient k(SII→SII) is expected to dominate the intercage process measured by the rate coefficient k(SII→W).[70] Intercage motions of adsorbate molecules through the 12-ring windows separating adjacent supercages are required for macroscopic species transport to occur, which is ultimately manifested as diffusion of guest molecules, such as benzene, within the nanoporous zeolite crystallite. Window adsorption sites are energetically less favorable and present a higher energy barrier to intercage benzene transport between supercages compared to the intracage SII-to-SII cation site hops examined here. Moreover, leaving a window site is expected to be much more facile than leaving a SII site; the corresponding mean residence time at the W site has been found in simulations[17a−d] to be orders of magnitude shorter than the mean residence time of benzene molecules at a Ca^{2+} SII site. Activation energy differences between intracage and intercage benzene hopping of 6 kJ mol^{-1} have been calculated for benzene adsorbed on Na-Y,[17d,23b] and even higher differences of about 15 kJ mol^{-1} have been obtained by T_1- and T_2-relaxation experiments on HY and US-Y.[23d] These results indicate that the correlation times for intracage vs. intercage motions differ by a factor of at least 10 over the temperature range investigated, making the slower intercage process very difficult to detect. First, only within a narrow temperature range (∼20 K) will the two processes both contribute to exchange intensity over the range of possible mixing times. Second, the intercage process is anticipated to contribute less than about 10% to the overall exchange intensity, which is on the order of the experimental scatter of the data. Third, the relatively fast spin diffusion in the benzene/Ca-LSX system can mask the slower dynamic process. Thus, the exchange ^{13}C NMR results from this study, together with corroborative molecular dynamics and Monte Carlo simulations,[17b−d,23b] and in conjunction with separate multiple-quantum ^{1}H NMR results,[59] present a consistent body of evidence that supports the predominance of intracage hops of benzene molecules among SII Ca^{2+} adsorption sites for low adsorbate loadings and at low/moderate temperatures.

(70) The window-to-window hopping rate coefficient k(W→W) is expected to be important only for high benzene loadings (>2 benzene molecules per supercage), when a sizable fraction of the W sites are occupied, or at elevated temperatures.

Summary and Conclusions

New applications of solid-state exchange ^{13}C NMR techniques to the study of hydrocarbon reorientation dynamics in nanoporous solids, specifically benzene molecules adsorbed on Ca-LSX zeolite, have yielded detailed quantitative insight on discrete molecular transport processes that are central to the adsorption and diffusion properties of heterogeneous host−guest systems. Two-dimensional exchange NMR spectra and time-domain-stimulated echo signals were used to examine the geometry of benzene hopping motions among adsorption sites in Ca-LSX. Distributions of jump angles about the two mean values of 0° and 109° were found, described by approximate Gaussian distributions of reorientation angles with widths of 5°−15° (fwhm). Variable-temperature measurements of 1D EIS ^{13}C NMR spectra have enabled the motional correlation times and apparent Arrhenius activation energies of benzene hopping between adsorption sites to be obtained directly from the experimental data. Two processes contribute exchange intensity to the experimental EIS spectra: site-hopping of benzene molecules among adsorption sites and spin diffusion among ^{13}C nuclei. Accurate measurement of the spin-diffusion rate constant allows for precise determination of the motional rate coefficient, $1/\tau_M$, which, in turn, is closely related to k(SII→SII), the rate for intracage hopping between Ca^{2+} SII adsorption sites. For the low loading range investigated, no significant adsorption of benzene in the 12-ring windows connecting adjacent supercages is expected nor observed within the sensitivity of the measurements. Furthermore, on the basis of MD simulations the rate coefficient k(SII→W), characterizing intercage hopping of benzene molecules into window sites between adjacent supercages, is expected to be a factor of 10 smaller than k(SII→SII). Inferring the motional parameters obtained from spin−lattice relaxation times T_1, spin−spin relaxation times T_2, or the analysis of solid-echo line shapes always requires a model for the motional process under study and generally an involved analysis to obtain information on the motional time scale. This is in contrast to the analysis of the exchange NMR experiments presented here, which yield model-free information about the geometry and time scale of the reorientational dynamics directly from the experimental data. This holds even in the presence of spin diffusion, which can be quantitatively taken into account to obtain accurate kinetic measurements of the molecular site-hopping process. Overall, exchange NMR presents a significantly more direct approach to the study of molecular length scale (10^{-9} m) transport events in heterogeneous porous solids than relaxation time measurements and are complementary to PFG NMR experiments, which probe diffusion on longer length scales (> 10^{-6} m).

Typical reorientation rate coefficients for benzene site-hopping in Ca-LSX at room temperature range from 5 to 25 s^{-1}; apparent activation energies are determined to be 66 ± 6 kJ mol^{-1} for the loading range (≤2 benzene molecules per supercage) investigated, with Arrhenius prefactors established to be about 1×10^{12} s^{-1}. These values are known or expected to depend on numerous local structural factors and conditions, including cation composition, adsorbate loading and siting, framework composition and architecture, adsorbate species structure and concentration, temperature, pressure, etc., which are currently under investigation in our laboratory. The interrelated nature of these synthesis and process variables is responsible for the complicated macroscopic adsorption, diffusion, and catalytic properties of heterogeneous molecular sieve materials. The quantitative molecular measurements presented here advance the prospects for establishing the molecular origin of important transport and reaction properties of hydrocarbon

guest molecules in porous solids, with improved prospects for their control in these and other host−guest systems.

Acknowledgment. The authors thank Dr. C. G. Coe and Dr. J. E. MacDougall (Air Products and Chemicals, Inc., Allentown, PA) for kindly providing Ca-LSX material used in the 2D exchange experiments, Professor S. M. Auerbach, Professor H. I. Metiu, and Professor K. Schmidt-Rohr for stimulating discussions, and are indebted to Dr. S. Wefing for helpful advice in the simulation of the structure factor curves. Support is gratefully acknowledged from the U.S. National Science Foundation under the Young Investigator program (DMR-9257064), using instrumentation and facilities supported by the NSF Division of Materials Research under grant DMR-9222527, and through the NSF-UCSB Materials Research Laboratory (MRL) program under Award No. DMR-9632716. Partial support has also been provided by the Shell B.V. and the David and Lucile Packard Foundation. B.F.C. is a Camille and Henry Dreyfus Teacher−Scholar and an Alfred P. Sloan Research Fellow.

JA971563M